Mémoire

Auteur : Samar Abdelmohsen Elsayed Youssef Talkhan,
Promoteur(s) : Wilmotte, Annick; Christodoulou, Maria
Faculté : Faculté des Sciences
Diplôme : Master en biologie des organismes et écologie, à finalité approfondie
Année académique : 2024-2025
URI/URL : http://hdl.handle.net/2268.2/23861

Research Unit: InBios – Center for Protein Engineering
Public Collection: BCCM/ULC – Cyanobacteria Collection

Faculty of Sciences
Department of Biology, Ecology and Evolution

Taxonomic Insights into *Nostoc*: Integrating a Polyphasic Approach for the Identification of Novel Species and a New Genus from Polar and Temperate Ecosystems

Master thesis presented by Samar Talkhan

Submitted for the degree of Master in Biology of Organisms and Ecology, *finalité approfondie*.

August 2025

Supervisor: **Dr. Annick Wilmotte**

Co-Supervisor: **Maria Christodoulou**

Acknowledgment

I would first like to express my deepest gratitude to my thesis promoter, Dr. Annick Wilmotte, for giving me the opportunity to conduct this research within the esteemed BCCM/ULC collection. Her leadership and the scientific environment she fosters at the InBios research unit were fundamental to this project.

My most sincere thanks go to my co-supervisor, Maria Christodoulou, for her invaluable guidance, and immense support throughout every stage of this work. Her expertise was essential, and this thesis would not have been possible without her dedicated involvement day after day.

I am also deeply grateful to the entire BCCM/ULC team and the technicians for their technical support, insightful advice, and for creating such a stimulating and collaborative atmosphere in the laboratory.

I extend my thanks to the University of Liège and the Department of Biology, Ecology, and Evolution for providing the academic framework and resources necessary for this Master's thesis.

Finally, a special thank you to my family and friends for their unconditional support, endless encouragement, and understanding throughout this academic journey.

Abstract

The genus *Nostoc* is a ubiquitous and morphologically complex group of cyanobacteria that thrive in a remarkable diversity of freshwater, terrestrial, and extreme environments. However, its taxonomy remains problematic and heterogeneous owing to its historical reliance on morphological characteristics, resulting in over 300 described species and a polyphyletic genus structure, necessitating modern molecular evaluation. To address these challenges, this study applied a polyphasic approach to classify thirteen cyanobacterial strains from the BCCM/ULC collection at the University of Liège. The methodology included morphological characterization via light microscopy, PCR amplification and sequencing of the 16S rRNA gene and the 16S–23S ITS region, phylogenetic analyses, evaluation of 16S rRNA sequence similarity, and assessment of ITS sequence dissimilarity along with secondary structures of conserved regions (D1-D1', Box-B, V3 helices). The results indicated significant cryptic diversity, with several strains likely representing novel species within the *Nostoc sensu stricto* clade and a novel genus closely related to *Nostoc*. This study highlights the necessity of the polyphasic approach in cyanobacterial taxonomy and pinpoints the ongoing challenges in cyanobacterial systematics.

Résumé

Le genre *Nostoc* est un groupe ubiquiste et morphologiquement complexe de cyanobactéries qui prospèrent dans une remarquable diversité de milieux d'eau douce, terrestres et extrêmes. Cependant, sa taxonomie demeure problématique et hétérogène en raison de sa dépendance historique aux caractéristiques morphologiques, ce qui a conduit à la description de plus de 300 espèces et à une structure de genre polyphylétique, rendant nécessaire une évaluation moléculaire moderne. Pour relever ces défis, cette étude a appliqué une approche polyphasique pour classifier treize souches de cyanobactéries issues de la collection BCCM/ULC de l'Université de Liège. La méthodologie incluait la caractérisation morphologique par microscopie optique, l'amplification par PCR et le séquençage du gène 16S rRNA et de la région ITS 16S–23S, des analyses phylogénétiques, l'évaluation de la similarité des séquences 16S rRNA et l'examen de la dissimilarité des séquences ITS ainsi que la structure secondaire des régions conservées (hélices D1-D1', Box-B, V3). Les résultats ont révélé une grande diversité cryptique, plusieurs souches représentant probablement de nouvelles espèces au sein du clade *Nostoc sensu stricto* et un genre nouveau étroitement apparenté à *Nostoc*. Cette étude souligne la nécessité de l'approche polyphasique dans la taxonomie des cyanobactéries et met en évidence les défis persistants de la systématique de ce groupe.

List of figures

List of tables

List of abbreviations

gDNA	Genomic DNA
SSU rRNA	Small subunit ribosomal RNA
Bp/kb	Base pair/Kilobase
Nt	Nucleotide
ITS	Internal Transcribed Spacer
RuBisCO	S-ribulose 1,5-biphosphate carboxylase-oxygenase
BCCM	Belgian Coordinated Collections of Microorganisms
ULC	University of Liège Cyanobacteria Collection
PCR	Polymerase Chain Reaction
RT	Room Temperature
TBE	Tris-Borate-EDTA
BLAST	Basic Local Alignment Search Tool
NCBI	National Center for Biotechnology Information
BI	Bayesian Inference
MCMC	Markov Chain Monte Carlo
PSRF	Potential Scale Reduction Factor
hc	Heterocytes
ML	Maximum Likelihood
MQ	Milli-Q

Table Of Contents

1 Introduction

Cyanobacteria (i.e., cyanophytes, cyanoprokaryotes) are old prokaryotic phototrophic microorganisms (Komárek, 2010b). They represent a diversified bacterial phylum with complicated morphologies, and extensive ecological amplitude (Dvořák et al., 2015).

They were the earliest organisms to evolve a two-step photosynthetic process that photolyzed water, and generated molecular oxygen. This innovation led to the Great Oxidation Event approximately 2.4 billion years ago, marking one of the most important shifts in Earth's history (Bekker et al., 2004). This fundamental environmental transformation established the crucial condition to the later emergence, and evolutionary diversification of more complex, aerobic life forms (Demoulin et al., 2019; Wilmotte, 1994).

Furthermore, their presence from the Precambrian era to the present day demonstrates their remarkable ecological and biological adaptability and success (Komárek, 2016).

Cyanobacteria constitute a dominant group within phytoplankton communities and serve a critical function in global biogeochemical cycles, particularly in mediating carbon, nitrogen, and phosphorus fluxes (Willis et al., 2022). Exhibiting remarkable morphological, phylogenetic, and functional diversity among bacterial phyla, their ecological adaptability allows them to thrive in a wide range of environments, including freshwater, marine, and terrestrial ecosystems. This adaptive capacity extends to extreme habitats, with populations thriving across polar regions to equatorial zones (Willis et al., 2022).

The cryosphere (i.e., Arctic, Antarctica, and alpine ecosystems) presents particularly challenging conditions for life due to persistent subzero air temperatures, limited liquid water availability, and high UV radiation exposure. Additionally, these regions experience extreme seasonal light variations, ranging from total darkness in winter to 24-hour sunlight in summer. Despite these combined stressors, cyanobacteria have demonstrated adaptable strategies and serve as keystone organisms in these extreme habitats, executing critical ecological functions (Whitton, 2012).

In our study, we focus on the *Nostoc* genus, a filamentous cyanobacterium that forms colonies ranging from microscopic to visible sizes and which is found in both terrestrial and aquatic environments (Komárek, 2013).

Despite its ubiquity, the taxonomy of *Nostoc* remains challenging due to the lack of distinctive morphological features and complex life cycle (Komárek, 2010b).

The application of polyphasic approaches for cyanobacterial classification over the past few decades has led to the description of numerous novel cyanobacterial genera and species. This method combines morphological, ecological, and molecular characteristics, providing a comprehensive means of addressing the persistent taxonomic challenges posed by the genus *Nostoc* (Komárek, 2016).

1.1 Historical taxonomy of cyanobacteria

As noted by (Komárek, 2016), the classification of cyanobacteria has evolved thought distinct historical periods, each defined by the prevailing methodological approaches of the time. From Linnaeus to the 20th century, cyanobacteria were studied by phycologists, who developed identification keys, and illustrated guides to facilitate their classification (Komárek, 2013). Geitler (1932), was the first to consolidate the classical taxonomic framework, commonly known as the 'Geitlerian approach'. This system based on the morphology of field-collected specimens, and traditional botanical criteria, was followed by many scientists afterwards according to Palinska & Surosz (2014).

Moreover, taxonomists were aware from the early stages of classification that relying solely on morphological characteristics observed through light microscopy was insufficient, especially for structurally simple organisms that also exhibit morphological variations in response to environmental changes (Sand-Jensen, 2014; Stanojković et al., 2022).

After that, in the second half of the 20th century, technological advances such as the electron microscope, and molecular methods revealed the structure, and function of many ambiguous features in cyanobacteria (e.g. cell wall structure, gas vesicle ultra-structure etc.) (Komárek, 2013).Based on these discoveries, it was clear that cyanobacteria should be studied as procaryotes (Stanier & Cohen-Bazire, 1977). At the same time, a new era for cyanobacterial taxonomy started by examining evolutionary relationships. This was especially important in morphologically flexible genera like *Nostoc*, where morphological features such as mucilage, filament fragmentation, and cell size change depending on environmental conditions. Because of that, relying solely on

morphology has often led to misidentifications, and overlapping species descriptions (Komárek, 2013).

In this context, the polyphasic approach which combines molecular data with morphological, ecological, and biochemical information has emerged as the most robust, and widely accepted framework for cyanobacterial classification (Cordeiro et al., 2020; Komárek et al., 2014). Within this framework, selecting appropriate molecular markers is crucial (Komárek, 2010a).

1.2 Molecular systematics in cyanobacteria

The small subunit ribosomal RNA (SSU rRNA) gene, known as the 16S rRNA gene in prokaryotes, has historically been an important marker in phylogenetic research. Introduced by Carl Woese, the 16S rRNA has significantly contributed to the identification of previously undescribed taxonomic groups. His research also justified the importance of the use of 16S, 5S, and 23S rRNA genes in bacterial systematics, based on their universality across prokaryotes (Doolittle, 1988).

The 16S rRNA gene, approximately 1500 bp in length, remains the most extensively used genetic marker in cyanobacterial studies. It enables the identification of closely related strains through sequence similarity, thereby assigning new sequences to the correct phylogenetic position within the cyanobacterial lineage (Kurmayer et al., 2017). Due to the presence of both conserved and variable regions, this gene is suitable for designing primers that can target either the entire phylum or specific cyanobacterial genera (Kurmayer et al., 2017), while its length allows deep phylogenetic and statistical analysis (Wilmotte & Golubic, 1991).

In this context, researchers have established various sequence similarity thresholds for this gene to distinguish between bacterial genera and species. At the species level, Stackebrandt & Goebel, (1994) first proposed a threshold of 97% for species separation based on a comparison of DNA-DNA reassociation values. It was modified to a threshold of 98.7–99% in 2006 after new experimental values were obtained (Stackebrand & Ebers, 2006). At the genus level, a threshold of 94.5%, was proposed by Yarza et al., (2014).

However, Fox et al., (1992) noticed that 16S rRNA marker alone cannot provide the resolution needed for prokaryotes at the species level. For example, in a study on Nostocaceae strains, the

concatenated 16S rRNA and ITS sequences revealed a well-supported monophyletic clade that was distinct from other phylogenetically and morphologically close strains, leading to the description of new species within the genus *Roholtiella*. In contrast, analyses based on 16S rRNA alone showed the species separation only weakly, with very short and poorly supported branches, highlighting the insufficiency of 16S rRNA alone for species-level resolution (Bohunická et al., 2015)

Thus, to enhance phylogenetic resolution among closely related taxa, scientists started using, along with the 16S rRNA marker, the internal transcribed spacer (ITS) between the 16S rRNA and 23S rRNA (Iteman et al., 2000; Wilmotte, 1994).

In cyanobacteria, the rRNA operon typically exists in multiple copies. The 16S–23S internal transcribed spacer (ITS) exhibits significant diversity in sequence composition, length, secondary structure, and the presence or absence of tRNA genes (Boyer et al., 2001). The 16S–23S rRNA spacer may include one or two tRNA genes ($tRNA^{Ala}$, $tRNA^{Ile}$) or both, or none (Iteman et al., 2000). Studies have reported that the ITS regions in cyanobacteria range between 354 and 1,012 nucleotides in length (Iteman et al., 2000; Rocap et al., 2002), and this region demonstrates greater variability compared to other molecular markers (Kurmayer et al., 2017).

Furthermore, the intragenomic variation is more pronounced in the ITS than in the 16S rRNA gene (Kurmayer et al., 2017), which make this region specifically useful for phylogenetic analyses for closely related species (Taton et al., 2006). While Wilmotte, (1994) argued that the high sequence diversity in cyanobacterial 16S–23S rRNA spacer regions complicates alignment, secondary structure analyses by (Iteman et al., 2000) revealed conserved domains (D1–D5), tRNA gene(s), and antiterminator boxes (A and B) within the ITS. These structural features facilitate alignment, particularly for distantly related species (Kurmayer et al., 2017).

Moreover, based on the work of Erwin & Thacker, (2008), strains within the same genus that show 0–3% dissimilarity in their 16S–23S ITS sequences are considered to belong to the same species, whereas values greater than 7% provide strong evidence for species separation. Intermediate values, between 3 and 7%, are regarded as ambiguous, and in such cases, the assignment of strains to the same or different species should be supported by morphological and ecological data (Christodoulou et al., 2023).

While the 16S rRNA and 16S–23S ITS regions have been widely used for resolving relationships among cyanobacteria, additional single-copy protein coding genes, such as *rbc*LX *and rpo*C1, have also proven valuable for supporting phylogenetic analyses and clarifying relationships among both closely and distantly related cyanobacterial groups (Iteman et al., 2000; Komárek, 2013).

The *rbc* operon, which includes genes for both S-ribulose 1,5-biphosphate carboxylase-oxygenase (RuBisCO) subunits (*rbc*S and *rbc*L), spans approximately 800-1000 base pairs (Kurmayer et al., 2017). Comparative genomic studies reveal that while the *rbc*L gene remains highly conserved across taxa, significant variation occurs in both the intergenic spacer and *rbc*X chaperone gene.

Apart from *rbc*LX, the *rpo*C1 gene (Palenik, 1994), which encodes the gamma subunit of the cyanobacterial RNA polymerase (Kurmayer et al., 2017), is a useful tool to complement 16S rRNA in clarifying the phylogenetic relationships of cyanobacteria, and can also be employed to resolve phylogenetic relationships among more distantly related cyanobacterial groups (Seo & Yokota, 2003).

In *Nostoc*, the use of *rpo*C1 and *rbc*LX genes as phylogenetic markers is constrained by the limited number of available sequences in public databases, restricting their broader application in taxonomic studies (Nowruzi et al., 2024).

1.3 Polyphasic approach

Molecular phylogenies have shown that most of the characters previously used to classify species are rarely synapomorphic (Mesfin et al.2020). On the other hand, describing species solely based on their separate positions on the phylogenetic tree, without considering morphological traits, prevents comparison with species described in the past through anatomical features for which molecular data are still unavailable (Komárek, 2020).

Another factor to consider is that, depending on the higher-level taxa, different traits in cyanobacterial genomes vary in terms of their stability, and taxonomic significance. As a result, the same characteristics may hold different taxonomic value depending on the clade (Komárek, 2016). Also, in various studies, and collections, the classification of cyanobacteria is based on arbitrarily selected morphological characteristics, leading to misapplied names, which complicates taxonomy of cyanobacteria (Komarek, 2006).

Moreover, in taxonomic evaluations, working with isolates may also present challenges. Cyanobacteria can undergo changes including altered morphology, altered physiological characteristics, and genotypes along with the subsequent loss of traits that resulted from adaptation to biotope conditions when they are transferred, and cultivated for an extended period of time under uniform conditions in collections, and labs (Komárek & Kaštovský, 2003).

To address these challenges in modern cyanobacterial classification, a polyphasic approach is used, one that integrates, and compares multiple relevant criteria to better define genetic, ecological, and morphological units across diverse environments. This method relies mainly on genetic data, while integrating additional diagnostic criteria, such as morphology, molecular, and ecological analysis (Casamatta et al., 2020; Komárek, 2016).

Moreover, the choice of supporting methods should be guided by the sample type, and an understanding of which traits best serve as reliable taxonomic markers (Komarek, 2006). This comprehensive approach is currently the most advanced method for accurately assessing cyanobacterial diversity (Komárek, 2020).

Also, it is important to note that the rapidly increasing number of genomic sequenced reference strains, has enabled the integration of phylogenetic analyses with traditional polyphasic taxonomy (Strunecký, 2023). The use of genomic data has now become a trend in the scientific community (Dextro et al., 2021); however, caution is needed, as many genera remain poorly represented or entirely absent from public sequence databases (Dextro et al., 2021, 2024).

The Belgian Coordinated Collections of Microorganisms (BCCM) is a consortium uniting seven biological resource centers, each with complementary expertise. The Molecular Diversity and Ecology of Cyanobacteria Research Group, part of the InBios Research Unit at the University of Liège, is hosting the BCCM/ULC collection. This laboratory provides well-documented and authenticated cyanobacterial strains, and focuses on studying their diversity, ecological adaptations, and biogeography, with a particular emphasis on extreme environments such as polar regions. Among these are strains identified as *Nostoc*, whose confirmation requires the application of a polyphasic approach, combining morphological, ecological, and molecular analyses.

1.4 *Nostoc* genus: history, morphological characteristics and ecology

The *Nostoc* genus has fascinated humans for centuries. Its peculiar blue-green, gelatinous appearance sparked the imagination of many cultures, leading to a variety of colorful names. Some referred to it as "witch's jelly," "troll's butter," or even "sternschnuppen" (German for "shooting stars") (Potts, 1997).

The first documented references to *Nostoc* species trace back to China's Eastern Jin Dynasty (317–420 CE), when *Nostoc commune* called "*Ge-Xian-Mi*" formed part of the diet of the famous alchemist and hermit Hung Ge. The modern nomenclature, *Nostoc*, derives from the German-Swiss physician Paracelsus. The term "*Nostoc*" probably originated from linguistic hybrids of Old English ("**Nost**hryl" [nostril]) and German ("Nasenl**och**"). This etymology likely reflects the organism's characteristic mucilaginous morphology resulting from abundant extracellular polysaccharides (Potts, 1997).

Nevertheless, the genus was officially established and described by Bornet and Flahault in 1886, with *Nostoc commune* as the type species (Komárek, 2013). To date, more than 300 species of *Nostoc* have been described, and the majority most described between 1888 and 1992 relied solely on morphological characters (Komárek, 2013). This reliance led Komárek and colleagues to characterize *Nostoc* as taxonomically heterogeneous and stress the need for molecular tools (Komárek et al., 2014).

Nostoc species exhibit complex and unique lifecycles, during which the arrangement of filaments and the shape of the colonies may change (Komárek, 2013). According to the description of *Nostoc* Vaucher *ex* Bornet and Flahault, species of this genus have a complicated life cycle; their filaments are usually aggregated in gelatinous macro- or microscopic colonies, and cell shapes range from barrel-shaped to cylindrical. In addition to vegetative cells, in *Nostoc* (and within the order Nostocales in general), specialized vegetative cells can be observed, such as heterocytes and akinetes. Heterocytes develop when there is a lack of nitrogen and are involved in nitrogen fixation and the formation of hormogonia (Komárek, 2013).

Heterocytes are distinguished by thick cell walls, typically occurring in the middle or at the ends of the filaments, and are larger and paler than the vegetative cells. Another type of specialized cell is the akinete, a dormant cell that develops under unfavorable conditions and can germinate to produce new filaments (Komárek, 2013; Richmond, 2003).

Additionally, *Nostoc* produce hormogonia; short, motile trichomes that facilitate dispersal, and colonization of new habitats. Hormogonia are known as "infection units" during symbiosis with plants and are often induced by environmental cues (e.g., nitrogen deprivation, light shifts) (Risser, 2023). In the hormogenic cycle, hormogonia formation initiates through the fragmentation of aging vegetative filaments at sites next to heterocytes; following a period of motility and dispersal, these hormogonia will cease movement and differentiate into new vegetative filaments (Risser, 2023). In the sporogenic cycle, akinetes germinate, producing vegetative filaments (Hrouzek et at. , 2013).

Moreover, the sheath, a polysaccharidic, mucilaginous layer surrounding the trichomes or colonies (Whitton, 2012). It protects the cells from environmental stresses. The sheath serves multiple functions, it protects the organism from predation, concentrates metals, slows down gas exchange, and reduces water loss (Richmond, 2003; Seckbachet al., 2007).

Nostoc is widely distributed across diverse habitats, a success largely attributed to the remarkable ability of some strains to withstand desiccation and rapidly resume physiological activities such as photosynthesis and nitrogen fixation upon rewetting (Dodds et al., 1995; Richmond, 2003). This tolerance allows *Nostoc* to thrive in extreme environments, including polar regions, hot springs, deserts, and seasonally inundated wetlands or estuaries worldwide. For example, *Nostoc commune* dominates shallow temporary pools on limestone rocks from the tropics to polar areas (Richmond, 2003). In aquatic ecosystems, *Nostoc* is primarily benthic but can also form floating planktonic masses, and it has been documented in ultra-oligotrophic lakes, Antarctic and Icelandic lakes, high-altitude lakes, and even swimming pools (Dodds et al., 1995). Furthermore, *Nostoc* species often share habitats with various plants, bacteria, and actinomycetes. The soil in which *Nostoc* commonly grows tends to be strongly alkaline and rich in calcic deposits (Richmond, 2003). *Nostoc'*s strong coherence and water retention increase nitrogen and phosphorus concentrations while lowering acidity, contributing to soil amelioration; for instance, *N. sphaericum* is cultivated in rice paddies to enhance soil fertility (Dodds et al., 1995). Additionally, symbiotic cyanobacteria like *Nostoc,* form motile hormogonia, which are important for establishing associations with hosts. This includes bryophytes like *Anthoceros* (Adams & Duggan, 2008)*,* the angiosperm *Gunnera* (Johansson et al., 1992)*,* and fungal genera such as *Peltigera* (Rikkinen, 2013).

1.5 Nostoc polyphyly

Since the introduction of molecular methods into cyanobacterial classification, the systematics and taxonomy of cyanobacteria have been undergoing substantial changes (Casamatta et al., 2005; Dvořák et al., 2014), as many taxa were shown to be polyphylic (Hoffmann et al., 2004; Rajaniemi et al., 2005; Wilmotte & Herdman, 2001). In reaction, the strategy has been to establish smaller, clearly delineated genera through polyphasic characterization approaches (Komárek et al., 2014). Having a monophyletic genus with a limited number of species is better than having extensive, poorly defined polyphyletic genera that includes many distantly related species (Komárek et al., 2014).

Nostoc, is a famous example of a particularly taxonomically complex genus (Cai et al., 2019). Rudi et al., (1997) started the identification of *Nostoc* based on molecular phylogeny. After that, several phylogenetic analyses of 16S rRNA and ITS showed that the genus *Nostoc* was polyphyletic (Christodoulou et al., 2022; Rajaniemi et al., 2005).

From that point onward, many several strains which morphologically appears to be *Nostoc*–like, were split out of the core "*Nostoc sensu stricto*" clade and established new genera within Nostocaceae (Hentschke et al., 2017; Hrouzek et al., 2013; Řeháková et al., 2007).

Řeháková et al., (2007), isolated one strain from desert soil, where they found the new genus *Mojavia*. Afterwards, another new *Nostoc*-like genera were identified: *Desmonostoc* (Hrouzek et al., 2013), *Halotia* (Genuário et al., 2015), *Aliinostoc* (Bagchi et al., 2017) *Komarekiella* (Hentschke et al., 2017), *Compactonostoc* (Cai et al., 2019), *Roholtiella* (Bohunická et al., 2015), *Violetonostoc* (Cai et al., 2020), *Dendronalium* & *Amazonocrinis* (Alvarenga et al., 2021) and *Parakomarekiella* (Soares et al., 2021), *Purpurea* (Cai et al., 2020), *Pseudoaliinostoc* (Lee et al., 2021), *Minunostoc* (Cai et al., 2019).

However, despite all this effort, the taxonomic boundaries within the genus *Nostoc* remain unclear. This misclassification occurs due to the lack of distinct morphological features (Christodoulou et al., 2022), together with insufficient or incorrect reference sequences (Dvořák et al, 2018), and/or the absence of accompanying morphological descriptions, or even the use of misidentified specimens (Garduño-Solórzano et al., 2024), resulting in an artificial monophyletic grouping of *Nostoc* and *Nostoc*-like genera, and cause errors in nomenclature (Pham et al., 2025).

1.6 Objectives

The main objective of this study is to identify and classify thirteen new cyanobacterial strains from the BCCM/ULC collection using a polyphasic approach. The strains originate mostly from cold environments (Antarctica, Svalbard, Tyrol) but one was isolated in Belgium. This study will combine morphological, ecological and molecular methods: light microscopy for morphological characterization; PCR amplification and sequencing of the 16S rRNA gene, the 16S–23S ITS region; and phylogenetic analyses of the resulting sequences. Phylogenetic analyses will provide the primary molecular framework, and those molecular results will be integrated with morphological and ecological observations to determine the taxonomic placement of each strain.

2 Materials & methods

2.1 Cyanobacteria strains and cultivation conditions

Thirteen cyanobacterial strains initially identified as *Nostoc* sp. from the BCCM/ULC collection were used in this study. These strains were isolated from a range of cold environments, including freshwater and terrestrial niches in Antarctica (e.g., Prydz Bay, Sør Rondane Mountains), Norway as well as Italy and Belgium (see Table 1).

Liquid BG11 culture medium (Rippka, 1988) without nitrates (i.e., $BG11_0$) was used for strain cultivation. The culture medium was prepared following the protocol described in Appendix 1. The chemicals $K_2HPO_4 \cdot 3H_2O$, $MgSO_4 \cdot 7H_2O$, $CaCl_2 \cdot 2H_2O$, EDTA-$Na_2 \cdot 2H_2O$, $Na_2CO_3 \cdot 10H_2O$, $NaHCO_3$, and citric acid monohydrate were purchased from Merck (Darmstadt, Germany), whereas $ZnSO_4 \cdot 7H_2O$, H_3BO_3, $MnCl_2 \cdot 4H_2O$, $Na_2MoO_4 \cdot 2H_2O$, $CuSO_4 \cdot 5H_2O$, and $Co(NO_3)_2 \cdot 6H_2O$ were purchased from Carl Roth (Schoemperlenstr, Karlsruhe, Germany). Ferric ammonium citrate was purchased from Thermo Fisher (Erlenbachweg, Germany). The pH of the medium was then measured using the Orion Lab Star PH111 bench pH meter equipped with a GD9156BNWP double junction refillable epoxy-body pH electrode and was adjusted to 7 prior to sterilization using 0.1 N HCl aquatic solution. Following this step, 50 or 100 mL of $BG11_0$ culture medium were transferred to 100 mL- or 250 mL- Erlenmeyer flasks respectively and autoclaved at 121 °C for 15 min. All strains were grown under continuous illumination with white, fluorescent light at an intensity of 5–10 µmol photons m^{-2} s^{-1}, at 12 °C, 18 °C or room temperature (RT) for 60−90 days (see Table 1).

Table 1.

Nostoc sp. strains from the BCCM/ULC Cyanobacteria Collection, Including Their Culture Preservation Temperatures, Geographic Origins, and Isolation Habitats. [a]Room temperature

ULC number	Taxon name	Strain name	Temperature (°C)	Geographical origin	Isolation habitat	References
8	*Nostoc* sp.	ANT.LPR.1	12	East Antarctica, Prydz Bay	Lake Progress, microbial mat	Biondi et al., 2008; Cornet et al., 2021; Taton et al., 2006
16	*Nostoc* sp.	ANT.L52.5	12	East Antarctica, Prydz Bay	Lake 52, microbial mat	Biondi et al., 2008
38	*Nostoc* sp.	ANT.L52B.5	18	East Antarctica, Prydz Bay	Lake 52, microbial mat	Taton et al., 2006; Velichko et al., 2023
39	*Nostoc* sp.	ANT.L52B.6	18	East Antarctica, Prydz Bay	Lake 52, microbial mat	Biondi et al., 2008
46	*Nostoc* sp.	ANT.LG2.6	12	East Antarctica, Prydz Bay	Lake Gentner 2, microbial mat	Biondi et al., 2008; Muñoz-Martín et al., 2019; Pushkareva et al., 2018; Taton et al., 2006
50	*Nostoc* sp.	ANT.L34.1	18	East Antarctica, Prydz Bay	Lake 34, microbial mat	Biondi et al., 2008; Pushkareva et al., 2018; Taton et al., 2006
59	*Nostoc* sp.	ANT.L52B.8	18	East Antarctica, Prydz Bay	Lake 52, microbial mat	Jungblut, 2022; Martineau et al., 2013; Raymond et al., 2021; Taton et al., 2006
169	*Nostoc* sp.	OTC1	18	Dronning Maud Land, Sør Rondane Mountains	Utsteinen ridge, surface of soil close to OTC1	N/A
179	*Nostoc* sp.	OTC control	18	Dronning Maud Land, Sør Rondane Mountains	Surface of soil	N/A
423	*Nostoc* sp.	ANT.L36.1	12	East Antarctica, Prydz Bay	Lake 36, benthic microbial mat	Biondi et al., 2008; Taton et al., 2006
442	*Nostoc* sp.	214	18	Italy, Tyrol, Bolzano, Laas	Endolithic	N/A
619	*Nostoc* sp.	SV009	12	Arctic Norway, Svalbard	Sample taken on a bryophyte	N/A
632	*Nostoc* sp.	V21	RT [a]	Belgium, Clavier	Rocks and mud samples in a brook (Fontenoy)	N/A

2.2 Morphological characterization

Morphological characterization of the studied strains was performed using an Olympus BX43 light microscope (Olympus Corporation, Tokyo, Japan). Micrographs were captured using an Olympus SC100 camera and processed with cellSens Microscope Imaging Software (Olympus Corporation, Tokyo, Japan). Morphological characteristics, including trichome size, filament color, colony presence or absence, filament density, and trichome morphology (e.g., straight, flexuous, wavy, or screw-like), as well as trichome arrangement (e.g. solitary or associated), were observed and described. Sheath presence was assessed at 1000× magnification using IMMOIL-F30CC immersion oil Type F for microscopy (Olympus Corporation, Tokyo, Japan). The size, and shape of vegetative cells, heterocytes, as well as the position of heterocytes were examined. The presence or absence of hormogonia, presence or absence and position of akinetes was also assessed. These data were compared to descriptions available for *Nostoc* species and *Nostoc*-like genera.

2.3 Molecular characterization

2.3.1 DNA extraction

Genomic DNA (gDNA) was extracted from all samples using the DNeasy PowerLyzer PowerSoil Kit (Qiagen, Germany) following the manufacturer's protocol, with specific modifications. These were introduced to enhance mechanical cell lysis, and improve both DNA yield and purity for downstream applications. Initial processing involved pelleting biomass through centrifugation until a sufficient quantity was obtained (around 0.25 g of starting material). All steps described below were carried out at RT unless stated otherwise. Centrifugation was carried out in an Eppendorf 5424 centrifuge. The first modification included the addition of two different sizes of sterile acid-washed glass beads (213–300 µm and 425–600 µm; Merck, Darmstadt, Germany) into PowerBead tubes to enhance cell disruption. Then, the cyanobacterial biomass was added to the PowerBead tubes together with 750 µL of PowerBead solution and 60 µL of solution C1. The tubes were briefly mixed by vortexing and secured on a flat-bed vortex. The samples were vortexed for 22 min (modification 2) instead of 10 min; the combination of glass beads (mechanical lysis), PowerBead and C1 solutions (chemical lysis) allows the disruption of cell walls and release of cell content. Following this step, the tubes were centrifuged at 10 000 × *g* for 30 s. The supernatant was transferred to clean 2 mL collection tubes and 250 µL of solution C2 were added. The mixture was

briefly mixed by vortexing and incubated on ice for 10 min instead of 5 min at 2–8°C as described in the protocol (modification 3). After centrifugation at 10 000 × *g* for 30 s, up to 600 µL of supernatant were transferred to 2 mL tubes, and 200 µL of solution C3 were added. The mixture was again briefly mixed by vortexing and incubated on ice for 10 min instead of 5 min at 2–8°C as described in the protocol (modification 4). Following this step, the samples were centrifuged at 10 000 × *g* for 1 min and 700 µL of supernatant were subsequently transferred to clean 2 mL collection tubes; then 1200 µL of solution C4 (chaotropic solution) were added to the supernatant and mixed by inversion. After that, 600 µL of the supernatant was transferred to an MB spin column, centrifuged at 10 000 × *g* for 1 min, and the flow-through was discarded; this procedure was repeated 3−4 times for each sample. At this step, the DNA selectively binds to the MB spin column while contaminants pass through the filter membrane. The bound DNA was further washed by adding 500 µL of ethanol-based wash solution C5 to the MB spin column and subsequent centrifugation at 10 000 × *g* for 30 s. The flow through was discarded and the samples were centrifuged again at 10 000 × *g* for 1 min to completely remove ethanol from our samples. Each MB spin column was then transferred to a 2 ml collection tube and an additional 5-min incubation step with the lids open was introduced to the protocol to ensure complete ethanol evaporation (modification 5). At the last step, 100 µL of elution buffer C6 (10 mM Tris-HCl, pH 8.5) were added at the center of the membrane filter and an additional 5-min incubation step (modification 6). The tubes were then centrifuged for 30 seconds at 10 000× *g* and MB spin column was discarded. The eluted DNA was stored at –20 °C for future use.

The concentration and purity of the extracted DNA were assessed using a NanoVue Plus Spectrophotometer (GE Healthcare, Europe). Purity was determined based on both 260/280 and 260/230 absorbance ratios.

2.3.2 PCR amplification of 16S rDNA and ITS

The quasi-complete 16S rDNA region was amplified using the forward cyanobacteria-specific primer 16S359F 5’-GGGGAATYTTCCGCAATGGG-3’ (Nübel et al., 1997) and the universal primer 1492R 5'-TACGGYTACCTTGTTACGACTT-3’ (Lane, 1991) (Figure 1).

Amplification of the partial 16S rDNA region and the 16S–23S Internal Transcribed Spacer (ITS) region was carried out using the forward primer P5 5'-TGTACACACCGGCCCGTC-3'(Wilmotte et al., 1993), and the reverse primer 23S30R 5'-CTTCGCCTCTGTGTGCCTAGGT-3'(Taton et al., 2003), primers originally designed for cyanobacteria (Fig. 1)

Figure 1.

Diagram representing the operon for ribosomal RNA (rRNA) synthesis. ITS stands for Internal Transcribed Spacer between 16S and 23S. The primers used to amplify the 16S rRNA gene are shown in black, and those used to amplify the 16S-23S ITS region are shown in blue.

PCR reactions were performed in 50 µL reaction mixtures containing 1X TransTaq Hifi Buffer I (10× stock, containing 20 mM $MgCl_2$; TransGene, Biotech Co., Beijing, China), 0.2 mM of each deoxynucleotide triphosphates (dNTPs; Neo Biotech, France), 0.5 µM of each primer (Eurofins Genomics, Germany), 0.05 U of TransTaq HiFi DNA polymerase (5u/λ; TransGene, Biotech Co., Beijing, China), and 50-150 ng of genomic DNA, determined using NanoVue Plus Spectrophotometer (GE Healthcare, Europe). Each PCR run included a positive control, consisting of genomic DNA from the *Nostoc* strain ULC508 (previously extracted and successfully amplified), and two negative controls: a DNA extraction negative control (a blank extraction sample processed alongside the real samples) and a PCR reaction negative control (where DNA template was replaced with MQ water). Amplifications were performed in a Bio-Rad T100 thermal cycler, with the thermal cycling profiles provided below.

For the partial 16S rDNA gene, the thermal cycling profile included an initial denaturation step at 94 °C for 5 min, followed by 35 cycles of denaturation at 94 °C for 30 s, annealing at 57 °C for 30 s, and extension at 72 °C for 2 min, ending with a final extension at 72 °C for 7 min.

The thermal cycling conditions for the partial 16S rDNA and 16S–23S ITS region consisted of an initial denaturation at 94 °C for 5 min, followed by 35 cycles of denaturation at 94 °C for 30 s,

annealing at 55 °C or 57 °C for 30 s, and extension at 72 °C for 1 min, with a final extension step at 72 °C for 7 min.

To prevent contamination, especially by aerosols that can carry previous amplicons, strict precautions were applied during PCR work. The procedures were carried out in separate rooms: different pre-PCR rooms were used for DNA extractions and PCR setups, while post-PCR rooms were reserved for amplified products, which contain billions of DNA copies that can easily disperse through air or onto surfaces. Dedicated tools, including separate pipettes and filtered pipette tips, were used for each area. Work surfaces were regularly disinfected, and gloves were frequently changed to minimize the risk of contamination. In addition, a negative control was included in each DNA extraction set and PCR run and they were treated like other samples to detect possible contaminations.

2.3.3 Agarose gel electrophoresis

Genomic DNA, PCR products, and purified PCR products were analyzed on 0.8–2% w/v agarose gel depending on the length of the analyzed DNA fragment (0.8% w/v for gDNA, 1% w/v for the 16S rRNA, and 2% w/v for partial 16S–23S ITS region). For agarose gel preparation, the desired amount of agarose was transferred in a 250 mL Erlenmeyer flask containing 100 mL of 1x Tris-Borate-EDTA (TBE) buffer. The buffer was prepared from Tris (hydroxymethyl) aminomethane (TRIS) powder (VWR Chemicals BDH, Leuven, Belgium), boric acid (Carl Roth, Karlsruhe, Germany) and EDTA (Merck, Darmstadt, Germany); following the protocols described in Sambrook and Russell (2001), presented in Appendix 2. The mixture was then heated in a microwave to dissolve agarose. Following this step, the flask was carefully removed from the microwave and swirled very gently. The solution was cooled to 50–55 °C and 6 µL of Midori Green solution (Nippon Genetics Europe, Düren, Germany) were added. The agarose solution was swirled again, poured in the gel casting apparatus and allowed to solidify.

To load the gel, 40–60 ng of DNA (genomic, PCR, or purified PCR product), determined using NanoVue was mixed with 1/6 volume of 6X Loading Dye (Thermo Fisher Scientific, Erlenbachweg, Germany) and adjusted with MQ water to a final volume of 10 µL. The following DNA ladders were loaded on the gel as molecular weight references: the FastGene 1 kb Plus Ladder (Nippon Genetics) for genomic DNA and 16S rRNA amplicons, the Lambda DNA/HindIII Marker

(Thermo Fisher Scientific) for genomic DNA, and the FastGene 50 bp Ladder (Nippon Genetics) for the 16S-ITS amplicons. A volume of 5 µL of each ladder was loaded per well, according to the manufacturer's recommendations (Nippon Genetics; Thermo Fisher Scientific). The positive control (ULC508 strain, mentioned previously) was loaded alongside two negative controls: a PCR negative control (MQ water substituted for template DNA) to check for reagent contamination, and a loading negative control (MQ water with dye) to confirm the absence of contamination during the loading process.

The gel was then run at 70–75 V for 90–120 minutes, depending on the length of the DNA fragment/PCR product.

2.3.4 PCR and gel purification

The PCR products were purified using the NucleoSpin Gel and PCR Clean-up kit (Macherey-Nagel, Hoerdt, France), following the PCR clean up (16S rRNA) or DNA extraction from Agarose gels protocols (16S–23S ITS region) provided by the manufacturer was followed with some modifications. All steps mentioned below were carried out at RT unless stated otherwise. All centrifugation steps were carried out in an Eppendorf 5417R centrifuge. For PCR clean up, the first step consisted of adding 2 volumes of Buffer NTI to 1 volume of sample. The sample was then mixed by repeated pipetting, loaded onto a NucleoSpin Gel and PCR Clean-up column and centrifuged for 30 s at 11 000× *g*. The flow-through was discarded and700 µL of the ethanol-containing Buffer NT3 were added to the NucleoSpin Gel and PCR Clean-up column. Following this step, the samples were centrifuged for 30 s at 11 000 ×*g*. The flow through was discarded and the silica membrane of the column was washed with 700 µL of Buffer NT3 one more time. The flow through was discarded and the column was centrifuged for 1 min at 11 000 ×*g* to remove Buffer NT3 completely. The column was then transferred to a new, sterile 1.5 mL tube and left on the bench with open lids for 3−5 minutes to allow ethanol to evaporate (modification 1, not included in the manufacturer's protocol). Then, 40 µL of NE were added and incubated for 3 min (modification 2; step not included in the manufacturer's protocol). At the final step, the samples were centrifuged for 1 min at 11 000 × *g*. The eluate was reloaded into the column (modification 3; step not included in the manufacturer's protocol), incubated for 1 minute (modification 4; step not included in the manufacturer's protocol), and centrifuged again for 1 min at 11 000 × *g*. The

purity of the samples was confirmed by agarose gel electrophoresis. The purified PCR products were stored at −20 °C. The quantity and quality of the purified PCR products was evaluated using NanoVue Plus Spectrophotometer and agarose gel electrophoresis as described above.

When the presence of multiple ITS copies of different length was observed, it was needed to add a step of separation and extraction of the bands thanks to an agarose gel protocol. For this protocol, the entire volume of PCR reaction (50 µL) was mixed with 10 µL of 6X Loading Dye (Thermo Fisher Scientific, Erlenbachweg, Germany) and loaded onto a 2% agarose gel (Appendix 3). The gel run for 5–6 hours at 70 V, allowing the separation of the different ITS bands. The FastGene 50 bp and 1Kb DNA Ladder (Nippon Genetics Europe) were used to estimate fragment sizes. After electrophoresis, the agarose gel was transferred to a blue light transilluminator. Using a sterile razor blade, the desired fragments were sliced out and placed into labeled, pre-weighted 2 mL microcentrifuge tubes. The weight of the agarose slices was determined, and NTI buffer was added at a ratio of 4:1 (i.e. 400 µL of the NTI buffer for every 100 mg of agarose), according to the manufacturer's protocol. The tubes were then incubated in a water bath (VWR WB-2MS, Avantor, Stockholm, Sweden) at 55 °C for 15–20 minutes or until the agarose was completely dissolved; the samples were briefly mixed by vortexing every 2–3 minutes during the incubation period. After this step, the samples were loaded onto a NucleoSpin Gel and PCR Clean-up column and were purified following the same instructions as above.

2.3.5 Preparation of templates for Sanger sequencing

Before sequencing, the concentration and purity of the purified DNA products were assessed, and gel electrophoresis was performed, as described in section 2.3.3. Templates were then prepared according to the sequencing unit requirements.

Purified samples were sequenced at the Sequencing Unit of the GIGA Genomic Facility (University of Liège, Belgium), using the ABI3700 analyzer (Applied Biosystems, Waltham, MA, USA), and at Eurofins (Germany), using the BigDye Terminator v3.1 Cycle Sequencing Kit on an ABI 3730xl DNA analyzer (Applied Biosystems, Waltham, MA, USA). The sequencing reactions were performed using the same primers as the initial PCR amplifications: primers P5 and 23S30R were

used for the 16S-ITS region, and primers 16S359F and 1492R were used for the quasi-complete 16S rDNA region.

2.3.6 Sequence processing and quality control

The obtained ab1 files were inspected and edited in CodonCode Aligner v.9.0.1 (CodonCode Corporation, United States) to obtain consensus sequences. All bases exhibited Phred quality scores above 25. Consensus sequences were screened for chimeras using Pintail (Ashelford et al., 2005).

2.3.7 Phylogenetic analysis

The obtained 16S rRNA gene sequences were first evaluated for sequence similarity against publicly available cyanobacterial 16S rRNA sequences using the BLASTn tool in the NCBI database (Altschul et al., 1990). Additional nucleotide sequences from closely related species and genera (at least 1100 bp in length) were also retrieved from GenBank, creating a dataset of 214 taxa [with outgroup, *Synechococcus elongatus* PCC 6301 (NR_074309)]. All nucleotide sequences were aligned with ClustalX v2.1 (Larkin et al., 2007), followed by manual inspection and removal of ambiguous gaps. Sequence file conversion was performed using ALTER (https://www.sing-group.org/ALTER/, (Glez-Peña et aL., 2010). The best-fit nucleotide substitution models were selected based on the Akaike Information Criterion (Akaike, 1974) implemented in jModeltest v2.1.10 (Darriba et al., 2012). In addition to 16S rRNA-based phylogeny, two additional analyses (multilocus analysis including 16S rRNA + ITS, and ITS-based phylogenetic analysis) were performed. The phylogenetic analysis of ITS region was based on tRNA-containing ITS sequences of validly described *Nostoc* species. Unfortunately, *N. jammuense*, *N. coriaceum* and *N. breve* were excluded from this analysis; the ITS sequences of these species were incomplete and of poor quality, which prevented the correct alignment of the ITS region. For the 16S rRNA-ITS multilocus analysis, a 665 bp-long segment of ITS was concatenated with the corresponding 16S rRNA gene sequence (1086 bp-long) using Concatenator v.0.2.1 (Vences et al., 2022). The GTR + I + G substitution model was selected for both 16S rRNA and ITS region.

Bayesian Inference (BI) analyses were performed using MrBayes v3.2.7a (Ronquist et al., 2012) on the supercomputers of the IT Centre for Science – CSC (Finland). For the 16S rRNA

phylogenetic analysis, two runs with four chains each (one cold and three heated) were conducted simultaneously for 25×106 Markov Chain Monte Carlo (MCMC) generations starting with a random tree. Both ITS and multilocus analyses involved two runs of 5×10^6 MCMC generations. Trees were sampled every 1000 generations in all runs. The average standard deviation of split frequencies between the two MCMC runs was below 0.01 and the potential scale reduction factor (PSRF) value for all estimated parameters was 1.00. The first 25% of trees were discarded as burn-in and a 50% majority rule consensus tree including posterior probabilities was calculated. ML analyses for all datasets were conducted using IQ-Tree v1.6.12 (Nguyen et al., 2015), employing the same nucleotide substitution models and 1000 bootstrap replicates. Phylogenetic trees were visualized with FigTree v1.4.2 (Rambaut, 2007) and redrawn using Inkscape v0.48.4 (The Inkscape team, 2020).

A similarity matrix (p-distance) for the 16S rRNA dataset was generated using MEGA 7 (Kumar et al., 2016).

2.3.8 Analyses of the secondary structure of 16S–23S Internal Transcribed Spacer (ITS)

The ITS regions were identified manually following Iteman et al. (2000). To detect the presence and position of tRNA genes, we used tRNAscan-SE [https://lowelab.ucsc.edu/tRNAscan-SE/index.html; (Lowe & Chan, 2016)]. Hypothetical secondary structures of D1–D1', box B and V3 helices were predicted using Mfold web server [https://www.unafold.org/mfold/applications/rna-folding-form.php; (Zuker, 2003)] with default settings, except the structure drawing mode, which was set to "Untangle with loop fix". Among the predicted structures, those with the lowest Gibbs free energy (ΔG) were selected as the most thermodynamically stable conformations. The predicted structures were compared to available homologous structures from validly described species of *Nostoc* containing both tRNA-Ile and tRNA-Ala as well as genera that were phylogenetically close to the strain "*Nostoc*" sp. ULC619. The length (bp) of each region was also recorded and ITS sequence percent dissimilarity matrix was calculated in MEGA 7. Although the non tRNA-containing operons were obtained for all ULC strains, their comparison with other validly described species was not possible due to lack of available comparable data in GenBank.

3 Results

3.1 Morphology

ULC 8 (Fig. 2)

In liquid media, the trichomes were either solitary or in clusters, they were always found at the bottom of the culture flask but were never attached to the surfaces of the culture flask. Trichomes were cylindrical, uniseriate, long, flexuous, irregularly entangled, non-motile and without false branching, always surrounded by a common soft, gelatinous, colorless mucilage, 3.40–4.28 µm in width, constricted at the cross-walls. Cells were subspherical to compressed spherical, green in color 3.40–5.00 µm long and 3.40–4.28 µm wide. Heterocytes were spherical to subspherical 4.49–6.24 µm long and 4.34–5.87 µm wide. Reproduction occurred by hormogonia produced by trichome disintegration. Akinetes were not observed.

ULC 16 (Fig. 2)

In liquid media, the trichomes were either solitary or in clusters, they were found at the bottom of the culture flask, but were never attached to the surfaces of the culture flask. Trichomes were cylindrical, uniseriate, long, bent or coiled, 3.50–3.67 µm wide, without false branching, non-motile, constricted at the cross-walls. Vegetative cells were cylindrical to barrel-shaped 3.50–3.67 µm wide, with granular content. Heterocytes were ± spherical 4.44–6.33 µm wide, present at both intercalary and terminal positions. Reproduction occurred by formation of hormogonia. Akinetes were not observed.

ULC 38 (Fig. 2)

In liquid media, trichomes were either solitary or arranged in green to dark green clusters growing at the bottom of the culture flask. Trichomes were cylindrical, uniseriate, long, flexuous, variously curved, 2.91–3.11 µm wide, without false branching, non-motile, constricted at the cross-walls. As the culture senesced, trichomes become wider, gradually converting into akinetes. Vegetative cells were cylindrical, longer than wide, 2.91–3.11 µm in width, green in color and with granular content. Heterocytes were ± spherical to oval 4.81–7.02 long and 4.01–6.38 µm wide, occurring at both intercalary and terminal positions. Akinetes were observed. Reproduction was accomplished via hormogonia produced either by trichome disintegration or akinete germination.

ULC 39 (Fig. 2)

In liquid media, trichomes were either solitary arranged in green to dark green clusters growing at the bottom of the culture vessel. Trichomes were cylindrical, uniseriate, long, flexuous, variously curved, 3.50–3.72 µm wide, without false branching, non-motile, constricted at the cross-walls. As the culture senesced, trichomes become wider, gradually converting into akinetes. Vegetative cells were barrel-shaped, shorter than wide to isodiametric, 3.50–3.72 µm in width, green in color and had granular content. Heterocytes were ± spherical to oval 5.28–7.15 µm long and 4.70–6.50 µm wide, occurring at both intercalary and terminal positions. Reproduction occured via hormogonia produced either by trichome disintegration or akinete germination.

ULC 46 (Fig. 3)

In liquid media, the microcolonies formed a thin biofilm attached to the bottom of the culture flask. Microcolonies were elongate, spherical, sometimes of irregular shape, always surrounded by a thin, soft, smooth, colorless mucilage at all stages of the life cycle. Trichomes in young microcolonies were compact and densely arranged at first, becoming loosely arranged and growing distant from the outer margin during later stages of the life cycle. Free-living trichomes arising from hormogonia were always long, cylindrical, straight or bent at first, later variously curved, 2.89–3.50 µm in width and always constricted at the cross-walls. Vegetative cells are green in color, shorter than wide to isodiametric 2.89–3.50 µm wide and were granulated. Both terminal and intercalary heterocytes are of variable size and shape were observed, 3.34–5.23 × 3 µm long and .8–4.79 µm wide. Reproduction was accomplished via colony disintegration and release of young trichomes and by hormogonia produced by akinete germination

ULC 50 (Fig. 4)

In liquid media, thallus was green to dark green, thin, membranaceous, loosely attached to the surface of the culture flask. Microcolonies were either elongate, spherical or sometimes irregular, always surrounded by a thin, soft, smooth, colorless mucilage at all stages of the life cycle. Trichomes in young microcolonies were compact and densely arranged at first, becoming loosely arranged and growing distant from the outer margin of the sheath in later stages of the life cycle. Free-living trichomes arising from hormogonia were always long, cylindrical, variously curved or wavy, 4.06–4.79 µm in width and always constricted at the cross-walls. Vegetative cells were green

in color, cylindrical to oval 4.35–5.30 µm long and 4.06–4.79 µm wide with granular content. Both terminal and intercalary heterocytes varied in size and shape, were 4.97–6.31 µm long and 4.75–5.78 µm wide. Akinetes were present. Reproduction was accomplished via colony disintegration and release of young trichomes and via hormogonia produced by trichome disintegration or akinete germination.

ULC 423 (Fig. 4)

In liquid media, the microcolonies formed a thin biofilm of bright green to blue-green color attached to the bottom of the culture flask. Microcolonies were either spherical, spherical to oval or elongated, surrounded by a colorless mucilage. In young microcolonies, the trichomes were compact and densely arranged at first, becoming loosely arranged and growing distant from the outer margin at later stages of the life cycle. Free-living trichomes arising from hormogonia were always long, cylindrical, straight or bent at first, later variously curved, 3.67–5.26 µm in width, non-motile, without false branching, always constricted at the cross-walls. Vegetative cells, bright green to green in color when young, later turning olive green as the culture senesces, 3.67–5.26 µm wide. Heterocytes were mostly spherical, compressed spherical or spherical to oval, observed at both intercalary and terminal positions, 3.90–6.48 µm wide. Reproduction was accomplished via colony disintegration and release of young trichomes, via hormogonia and via akinete germination.

ULC 59 (Fig. 5)

In liquid media, the trichomes were either solitary or irregularly arranged in clusters of green to dark green color, loosely attached to the bottom of the culture flask. The trichomes were cylindrical, uniseriate, long, bent or flexuous, 3.25–3.68 µm wide, without false branching, motile (infrequent movement), constricted at the cross-walls. As the culture senesced, trichomes became wider, gradually converting into akinetes. Vegetative cells were cylindrical, usually shorter than wide to ± isodiametric, 3.25–3.68 µm in width, with granular content. Heterocytes were observed in both terminal and interacalary positions, having oval or spherical or subspherical shape, 4.52–7.53 µm long and 4.40–6.44 µm wide. Akinetes were observed. Reproduction occurred via hormogonia produced either by trichome disintegration or akinete germination.

ULC 179 (Fig. 5)

In liquid media, trichomes were either solitary or forming aggregates of dark green color, loosely attached to the bottom of the culture flask. Trichomes were cylindrical, uniseriate, long, straight, bent or variously curved, non-motile, 3.64–4.36 µm wide, without false branching, constricted at the cross-walls. Vegetative cells cylindrical, shorter than wide to isodiametric, 3.64–4.36 µm wide, greenish in color, sometimes with small granules. Heterocytes are mostly spherical or spherical to oval, 5.47–6.87 µm wide, observed mostly at intercalary positions, sometimes at terminal positions too. Akinetes present. Reproduction via hormogonia produced either by akinete germination or trichome disintegration.

ULC 442 (Fig. 6)

In liquid media, thallus was thin, membanaceous, subaerophytic, dark green in color. In young cultures, trichomes were long, cylindrical, straight, bent or variously curved, uniseriate, without false branching, 2.78–3.10 µm in width, non-motile. At this early stage of life cycle, cells were blue-green to greyish in color, not constricted at the cross-walls, bearing small granules. In aged cultures, trichomes were variously curved, sometimes coiled, dark green in color with wider cells (up to 4.0 µm in width) that will eventually convert into akinetes. Heterocytes at both intercalary and terminal positions were spherical or cylindrical in shape, 3.18–4.66 µm wide. Reproduction occurred by formation of hormogonia via trichome disintegration and akinete germination.

ULC 632 (Fig. 6)

In liquid media, filaments formed a thick mucilaginous mat of brownish to dark brown color. Filaments were long, cylindrical, flexuous and variously curved, irregularly arranged within the thallus. Sheath was very thin, colorless, always attached to the trichomes. Trichomes were long, cylindrical, uniseriate, 2.99–4.23 µm wide, non-motile and without false branching, not or slightly constricted at the cross-walls. Vegetative cells were cylindrical, 2.99–4.23 µm wide. Heterocytes were rarely observed at both terminal and intercalary positions, mostly oval-shaped 3.02–3.58 µm in width. Reproduction was accomplished by hormogonia formed via akinete germination or trichome disintegration.

ULC 619 (Fig. 7)

In liquid media, the filaments formed a mucilaginous thick mat of brown to brown-pink color. Trichomes were long, cylindrical, flexuous, variously curved 4.01–5.68 µm wide, sometimes surrounded by a wide, firm and colorless mucilage. Vegetative cells were subcylindrical to barrel-shaped (depending on the stage of the life cycle), brownish to brownish green in color, constricted at the cross-walls and had granular content. Heterocytes were observed at both terminal and intercalary positions, were 3.81–5.61 µm wide and were mostly spherical or subcylindrical. Akinetes were present. Reproduction was accomplished by hormogonia produced via akinete germination or trichome disintegration.

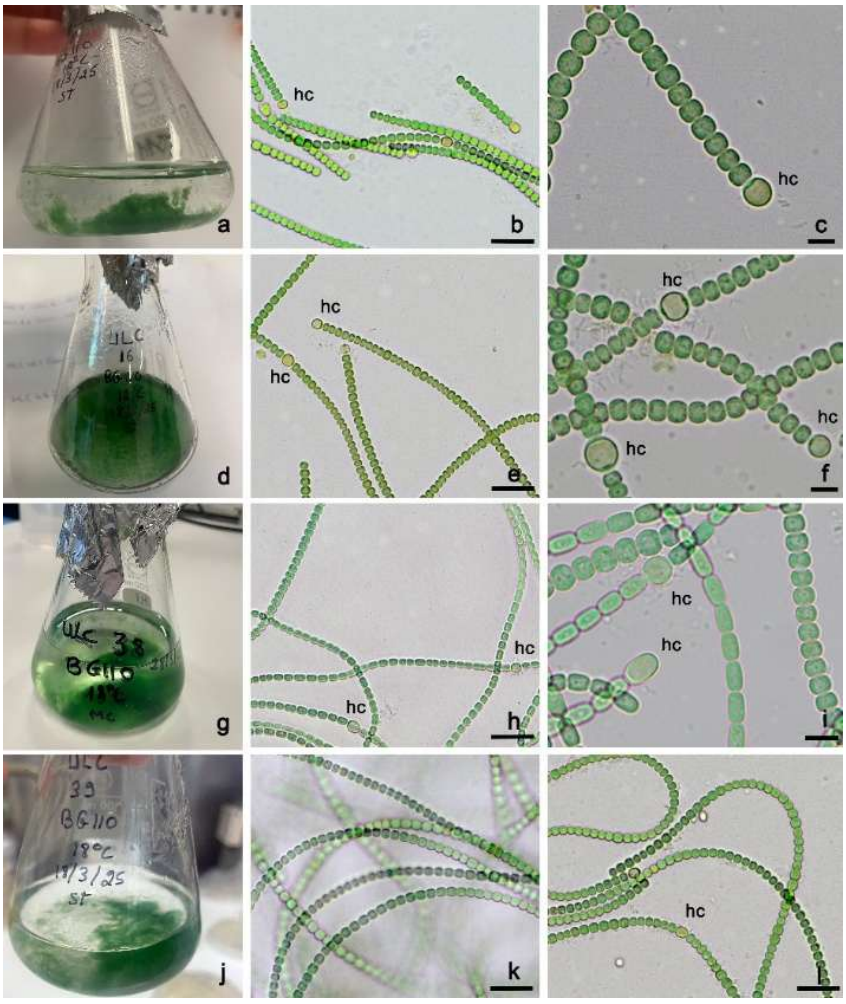

Figure 2. Culture morphology and light micrographs of strains ULC8, ULC16, ULC38, and ULC39 in $BG11_0$ medium. Cultures grew predominantly at the bottom of the vessel (a, d, g, j). Light micrographs show cylindrical, elongated trichomes with intercalary or terminal heterocytes (Hc) for ULC8 (b, c), ULC16 (e, f), ULC38 (h, i), and ULC39 (k, l). Scale bars: 20 µm (b, e, h, k, l); 5 µm (c, f, i).

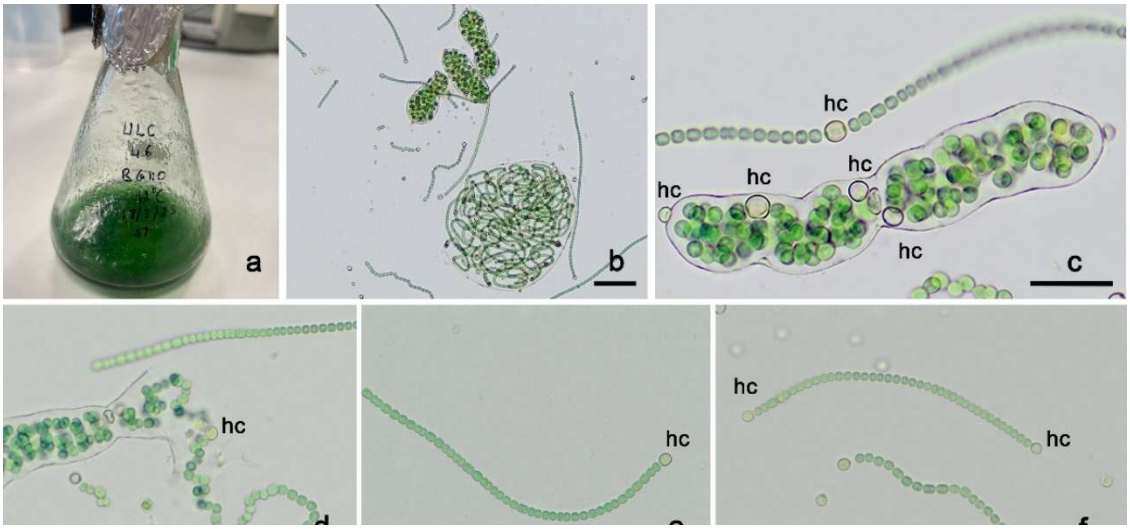

Figure 3. Culture morphology and life cycle of ULC46 microcolonies grown in $BG11_0$ medium. (a) Overall view of the culture attached to the flask. Under light microscope (b-f), (b-d) Microcolonies showing elongated and spherical (b) forms. Trichome organization progresses from compact and dense in young colonies (c) to loose in mature colonies (b), and subsequent trichome release (d). (e, f) Liberated trichomes are long and cylindrical. Heterocytes (hc) are present and variable in size and shape. Scale bars: 20 µm (c); 5 µm (b, d, e, f).

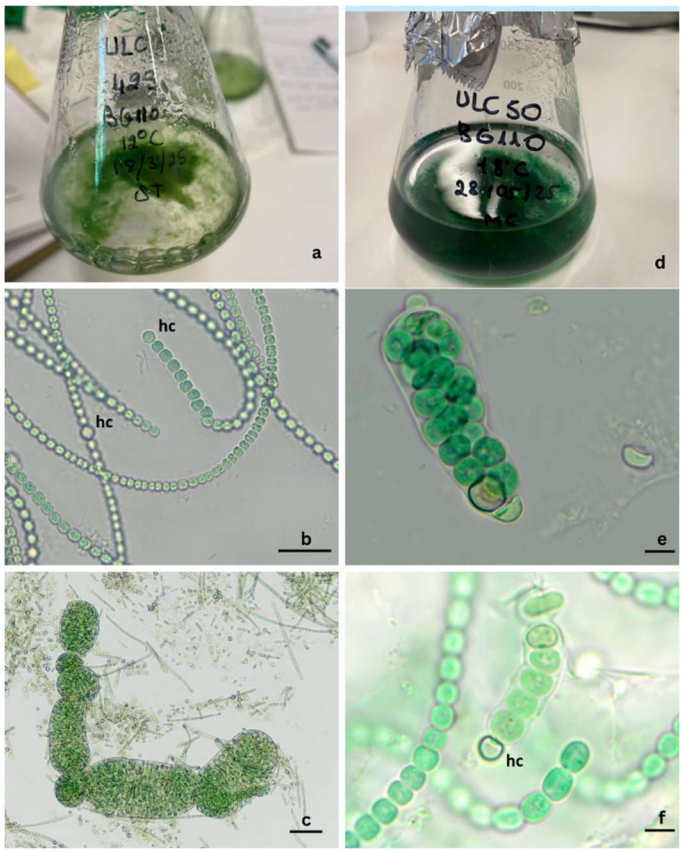

Figure 4. Culture morphology and light micrographs of ULC423, and ULC50**.** (a, d) macroscopic culture morphology in $BG11_0$ medium. ULC423 forms a thin, bright blue-green biofilm attached to the bottom (a), while ULC50 produces a dark green, loosely attached thallus (d). (b, c) Light micrographs of ULC423: (b) long, cylindrical trichomes; (c) spherical to elongated microcolonies. (e, f) Light micrographs of ULC50: (e) elongated microcolonies; (f) long trichomes. Heterocytes (Hc) are present in both strains. Scale bars: 20 µm (b); 50 µm (c); 5 µm (e, f).

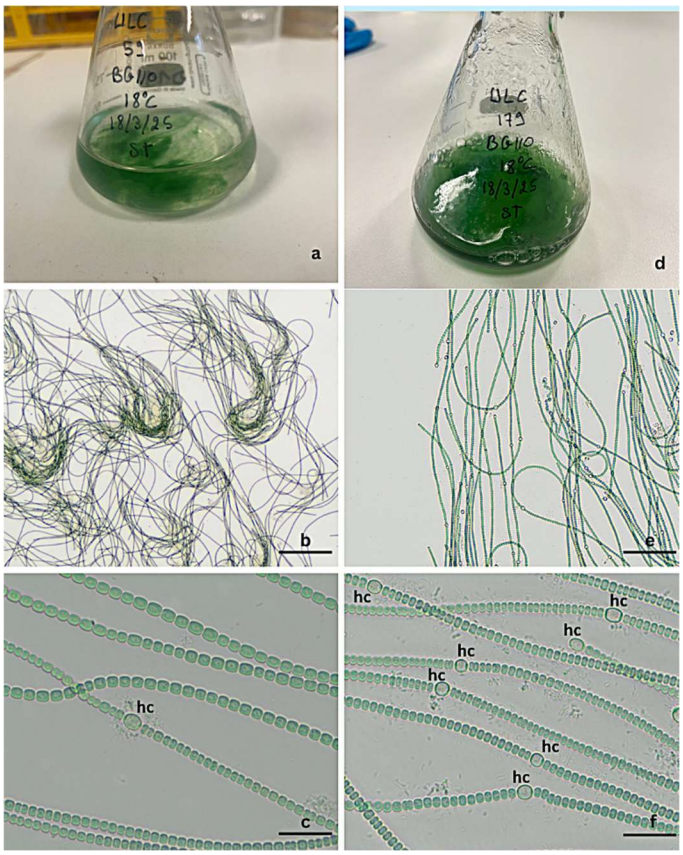

Figure 5. Culture morphology and light micrographs of strains ULC59 and ULC179 in $BG11_0$ medium. (a, d) macroscopic culture morphology. ULC59 trichomes are solitary or form loosely attached clusters (a), while ULC179 forms loosely attached, dark green aggregates (d). (b, c) Light micrographs of ULC59 show long, cylindrical trichomes, either solitary or in clusters. (e, f) Light micrographs of ULC59 show long, cylindrical trichomes. Heterocytes (Hc) are present in both strains. Scale bars: 20 µm (c-f); 50 µm (e); 200 µm (c, f).

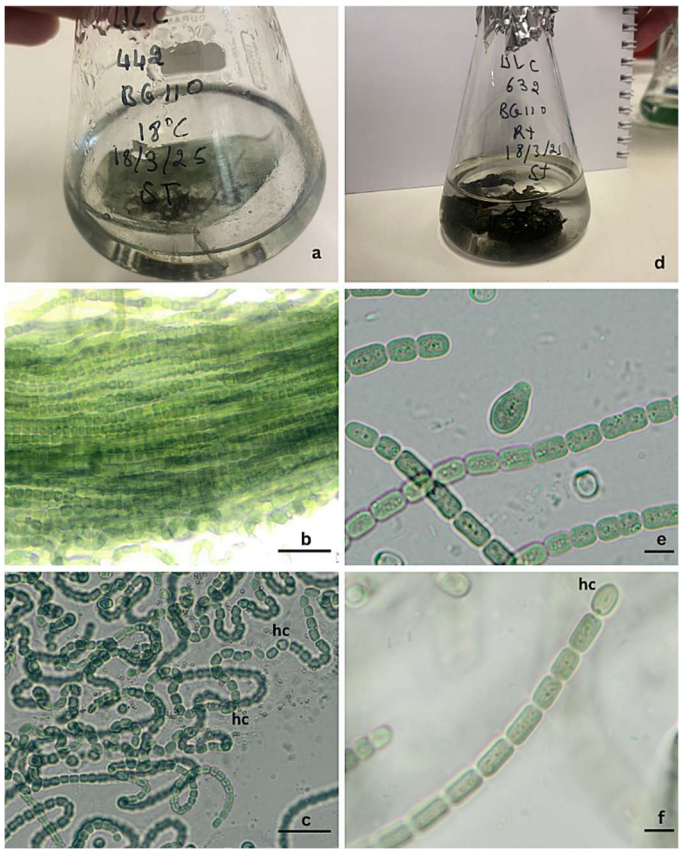

Figure 6. Culture morphology and light micrographs of strains ULC442 and ULC632 in BG110 medium. (a, d) macroscopic culture morphology. ULC442 forms a membranaceous, subaerophytic, dark green thallus (a). ULC632 forms a thick, mucilaginous, brown mat (d). (b, c) Light micrographs of ULC442 at different life stages: (b) blue-green trichomes in early growth; (c) dark green trichomes in later growth. (e, f) Light micrographs of ULC632 showing long, cylindrical trichomes and akinetes (e, f). Heterocytes (Hc) are present in both strains. Scale bars: 20 µm (b); 50 µm (c); 5 µm (e, f).

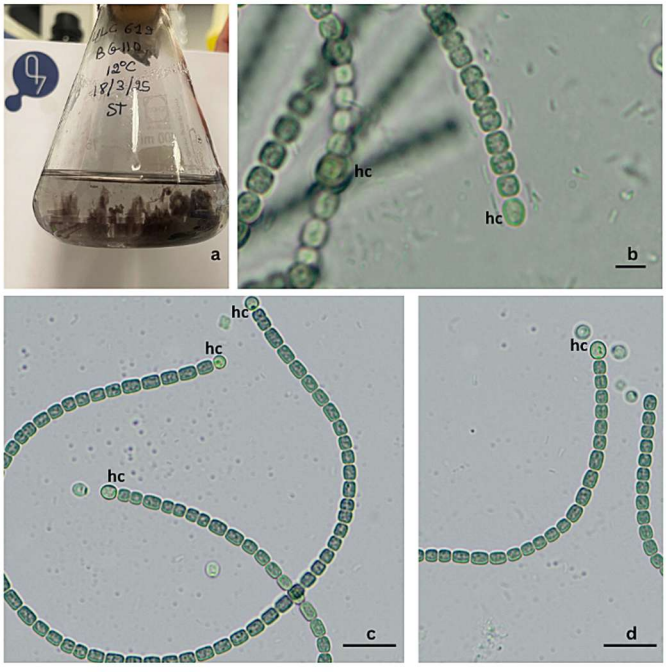

Figure 7. Culture morphology and light micrographs of strain ULC619 grown in BG110 medium. (a) macroscopic view showing a thick, mucilaginous, brown-pink mat. (b-c-d) Light micrographs revealing long, cylindrical trichomes with heterocytes (Hc) present in both terminal and intercalary positions. Scale bars: 20 µm (b-c-d).

3.2 Molecular studies

3.2.1 Genomic DNA extraction, quality, quantity

The nucleic acid concentrations across all samples ranged from 22.5 to 60.5 ng/µL (Table 2). The values recorded for $A_{260/280}$ ranged between 1.4 and 1.8, and $A_{260/230}$ ranged between 0.8 and 3.6. Agarose gel electrophoresis revealed a predominant DNA fragment of approximately 21 kb in length, alongside the expected smearing of fragmented genomic material (Fig. 8).

Table 2.

Nucleic Acid concentration (ng/µL) and Quality Ratios ($A_{260/280}$ and $A_{260/230}$)

ULC number	ng/µL	$A_{260/280}$	$A_{260/230}$
8	32.0	1.7	1.8
16	43.0	1.8	2.1
38	22.5	1.6	2.2
39	36.5	1.7	1.6
46	23.0	1.7	0.8
50	28.5	1.6	1.9
59	27.0	1.6	1.6
169	15.9	1.6	2,3
179	18.5	1.7	3.6
423	60.5	1.8	2.2
442	24.5	1.7	1.5
619	14.2	1.6	1.5
632	31.5	1.4	1.2

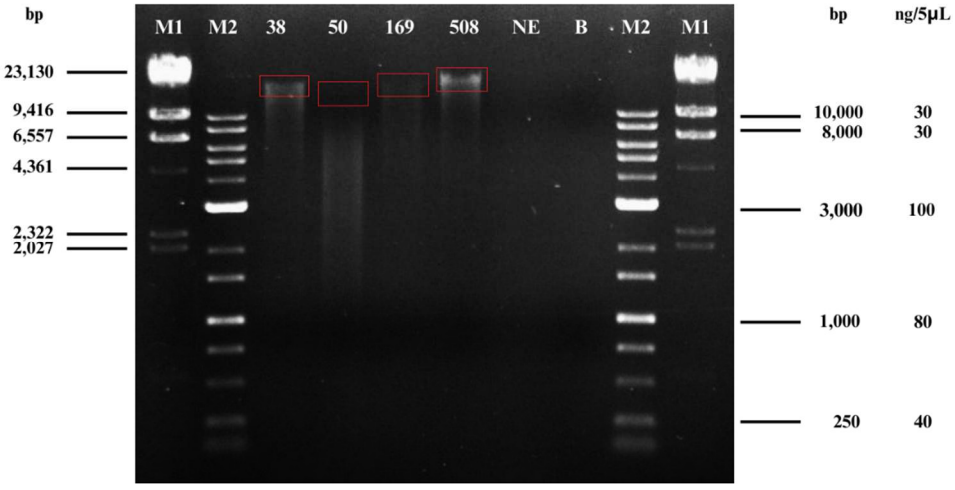

Figure 8. Agarose gel electrophoresis (0.8%) stained with Midori Green nucleic acid stain was performed for the extracted DNA. 5 µL of each extracted DNA sample were loaded per well. 38, 50, and 169 correspond to the studied strains and their respective ULC numbers, and 508 is the positive control. NE represents the extraction negative control, B is the blank lane (MQ water + dye), and M1 and M2 are DNA ladders (λ DNA HindIII and FastGene 1 kb, respectively). Electrophoresis was run for 2 h at 75 V.

3.2.2 PCR amplification and Purification

Both partial 16S rRNA gene and ITS region were successfully amplified in all samples (except ULC169). For 16S rRNA gene, all amplicons had a single band approximately 1200 bp long (Fig. 9). Two bands ~500 bp and ~750 bp were recorded for the ITS region (fig. 10).

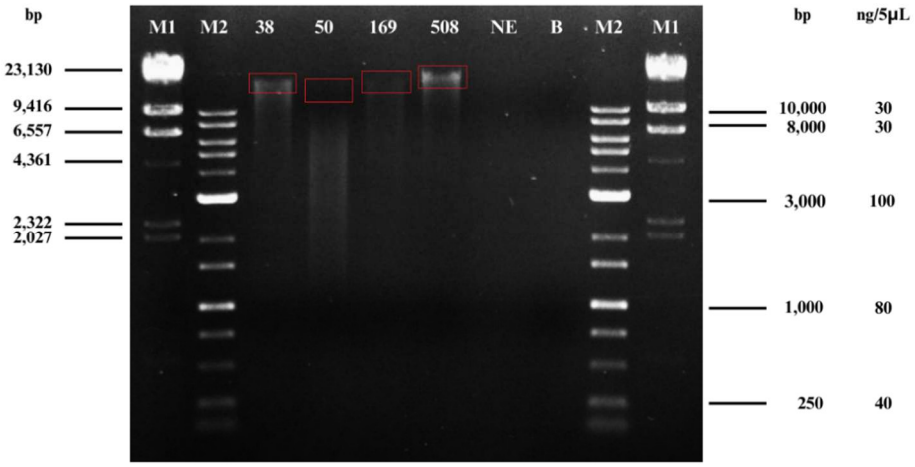

Figure 9. Agarose gel electrophoresis (1%) stained with Midori Green nucleic acid stain was performed for the 16S rRNA PCR products. 3 µL of each PCR product were loaded per well. Samples 423, 442, and 632 correspond to the studied strains and their respective ULC numbers, and 508 is the positive control. NE represents the extraction negative control, NP represents the PCR negative control, B is the blank lane (MQ water + dye), and M is the FastGene 1 kb DNA ladder. Electrophoresis was run for 2 h at 85 V.

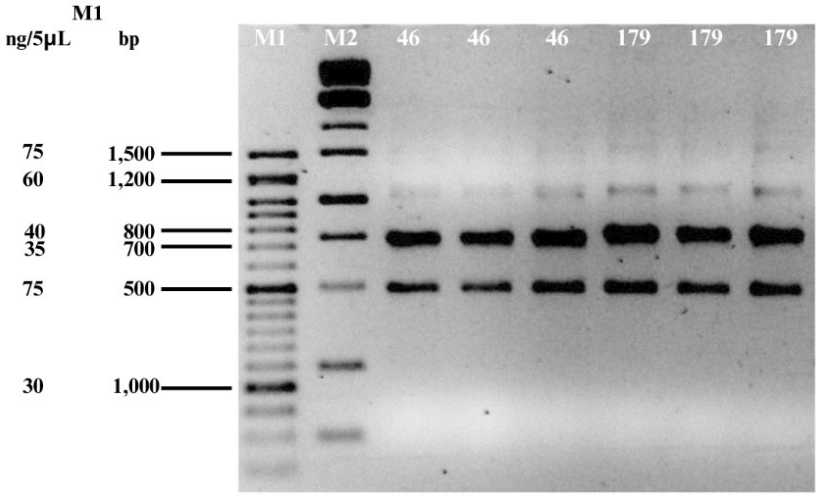

Figure 10. Agarose gel electrophoresis (2%) stained with Midori Green nucleic acid stain was performed for the 16S–23S ITS PCR products. 2 µL of each PCR product were loaded per well. Samples 46 and 179 correspond to the studied strains and their respective ULC numbers. M1 and M2 are DNA ladders (FastGene 50 bp and FastGene 1 kb, respectively). Electrophoresis was run for 2 h at 75 V.

All PCR products were successfully purified. For the 16S rRNA gene, nucleic acid concentrations across samples ranged from 107 to 181.5 ng/µL. For the 16S–23S ITS region, nucleic acid concentrations ranged between 8.7 and 53 ng/µL. The $A_{260/280}$ ratios varied between 1.55 and 1.77, and $A_{260/230}$ varied between 0.43 and 2.14 (Appendix 4).

3.2.3 Processing of ab1 files and consensus sequences

The length of the partial 16S rRNA nucleotide sequences for 12 out of 13 studied strains ranged between 1081 and 1118 bp. The complete 16S−23S ITS regions with and without tRNAs were recovered for these 12 strains except the tRNA-containing ITS region of strain ULC16 (partial sequence, lacking 18 nucleotides). The chromatograms of ULC169 for both 16S rRNA and the two ITS regions had bad quality. Further investigation led to the conclusion that this strain is not unicyanobacterial and it was not further processed.

3.2.4 16S rRNA phylogenetic analysis

A total of 214 taxa were included in the ML and BI analyses. Both analyses yielded nearly identical topologies and were mapped onto the same phylogenetic tree (Fig. 11).

Eleven studied strains were placed within the *Nostoc sensu stricto* clade. As seen in (Fig. 12), ULC8, ULC16, ULC38, ULC39, ULC59, and ULC179 (i.e. Group 1) clustered together and appeared closely related to *N. sikkimense* RESHI-1B-PS and *N. coriaceum* 34TNA-PS. Likewise, ULC50 and ULC423 (i.e. Group 2) clustered together whereas ULC46 clustered with *N. tlalocii* strains. ULC442 clustered with "*N. edaphicum*" CCNP1411 and Nostocales cyanobacterium Esc15.4. The strain ULC632 did not cluster with any other *Nostoc* strains. The abovementioned ULC strains shared 97.83 to 100% 16S rRNA sequence similarity with each other (Appendix 5).

The percent similarity between the *Nostoc* strains examined in this study and previously described *Nostoc* species ranged from 95.68 to 99.81% (Appendix 5). Specifically, group 1 showed 98.60–99.54% 16S rRNA sequence similarity with *N. commune* EV1-KK1, *N. punctiforme* PCC73102, *N. flagelliforme* IMGA0408, *N. edaphicum* X, *N. jammuense* (2JNA-PS and 21A-PS), *N. globosum* 4CHA-PS, *N. breve* BG11-PS, *N. coriaceum* 34TNA-PS, and *N. sikkimense* RESHI-1B-PS. The strain ULC46 displayed 97.93–98.78% 16S rRNA sequence similarity with *N. punctiforme* PCC73102 and *N. talocii*. Group 2 exhibited 98.51–99.26% similarity with *N. edaphicum* X, *N. punctiforme* PCC73102, *N. sikkimense* RESHI-1B-PS, *Nostoc* sp. Lukesova 40/93, and Nostocales cyanobacterium 2.7 (from Portugal). ULC442 shared 98.79–99.81% 16S rRNA sequence similarity with *N. commune* EV1-KK1, *N. punctiforme* PCC73102, *N. flagelliforme* IMGA0408, *N. edaphicum* X, "*N. edaphicum"* CCNP1411, *N. jammuense* (2JNA-PS and 21A-PS), *N. sikkimense*

RESHI-1B-PS, *Nostoc* sp. Lukesova 40/93, Nostocales cyanobacterium Esc15.4 (from a Spanish cave), *Nostoc* sp. CCAP 1453/28, *N. breve* BG11-PS, and Nostocales cyanobacterium 2.7. ULC632 shared 98.79–99.63% 16S rRNA sequence similarity with *N. globosum* 4CHA-PS, *N. breve* BG11-PS, *N. coriaceum* 34TNA-PS, *N. sikkimense* RESHI-1B-PS, as well as *N. commune* EV1-KK1, *N. punctiforme* PCC73102, *N. flagelliforme* IMGA0408, *N. edaphicum* X, and *N. jammuense* (2JNA-PS and 21A-PS).

ULC619 formed a highly supported monophyletic clade with Nostocales cyanobacterium L074_1_palm_4_1 and Nostocales cyanobacterium L013_1_Palm_2_12 (both isolated from the phyllosphere of laurel forests in the Canary Islands, Spain) (Fig. 11), with whom it shared 98.59 −98.88% 16S rRNA sequence similarity (Appendix 5). This clade was closely related to the genera *Kryptousia* (95.81−96.01% similarity), *Spirirestis* (95.42−96.01% similarity) and *Halotia* (96.11−97.08% similarity).

Figure 11. Maximum Likelihood (ML) phylogenetic tree based on 16S rRNA sequences of the studied strains together with 214 other cyanobacterial strains. Node labels indicate bootstrap values (≥50%) and posterior probabilities (≥0.50) derived from Maximum Likelihood and Bayesian analyses, respectively. Bootstrap values of 100% or posterior probabilities of 1.00 are marked with an asterisk (*), whereas bootstrap values <50% or posterior probabilities <0.50 are indicated with a dash (–). Studied species and genera are highlighted in bold red font. GenBank accession numbers are given in parentheses. The scale bar represents 0.08 substitutions per nucleotide position.

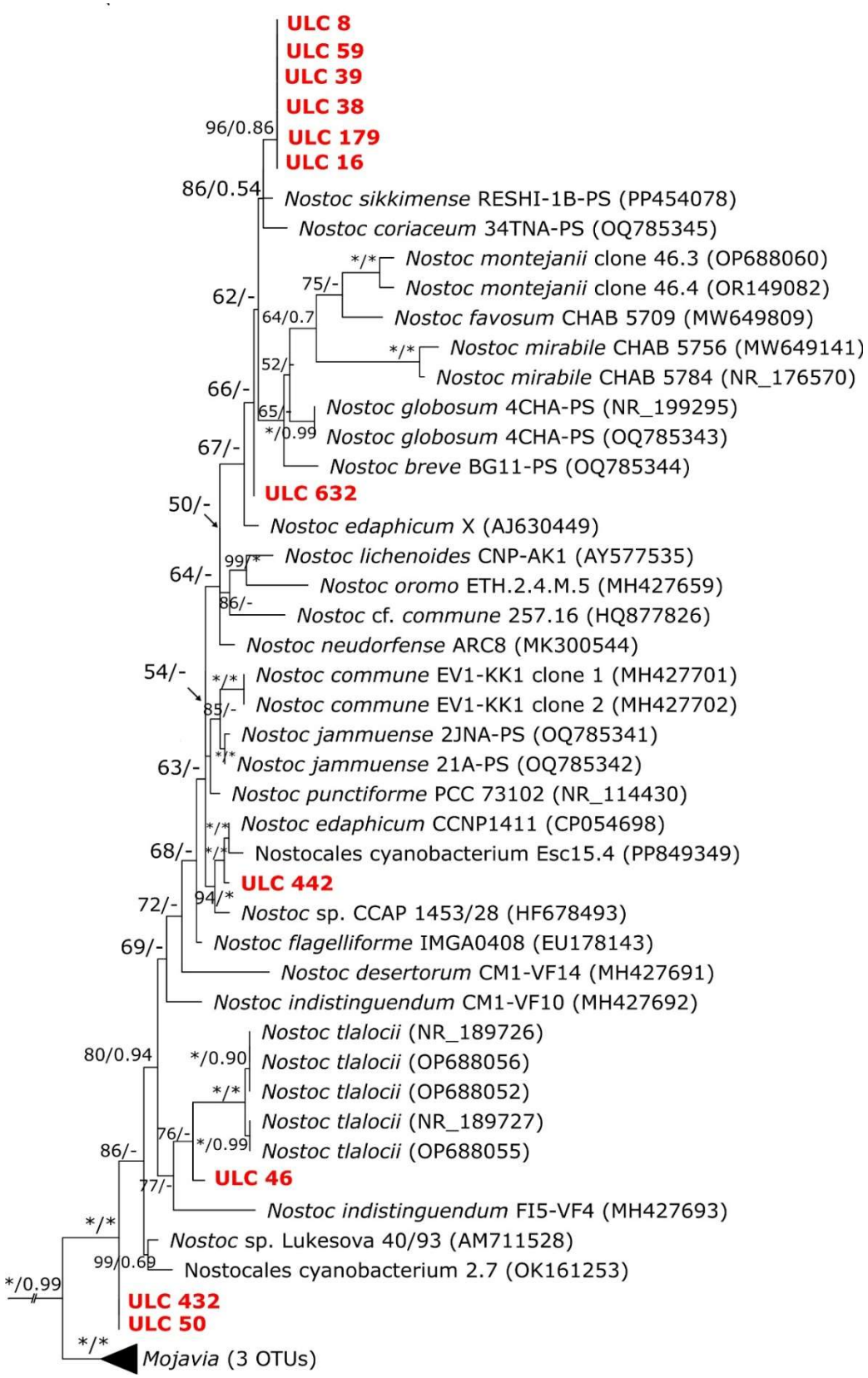

Figure 12. Maximum Likelihood (ML) phylogenetic tree based on 16S rRNA sequences of the studied Nostoc strains together with closely related taxa. Node labels indicate bootstrap values (≥50%) and posterior probabilities (≥0.50) derived from Maximum Likelihood and Bayesian analyses, respectively. Bootstrap values of 100% or posterior probabilities of 1.00 are marked with an asterisk (*), whereas bootstrap values <50% or posterior probabilities <0.50 are indicated with a dash (–). Studied species are highlighted in bold red font. GenBank accession numbers are given in parentheses.

3.2.5 ITS sequence phylogenetic analysis and comparison of secondary structures

The complete 16S−23S ITS region, containing both tRNAs, was obtained for all ULC strains except ULC16 (partial sequence).

As seen in Figure 13, ULC632 clustered with *N. punctiforme* PCC 73102, while ULC442 clustered with *N. edaphicum* CCNP1411. On the other hand, ULC423 grouped together with ULC50 and was closely related to *N. desertorum* CM1-VF14. In contrast, ULC strains 8, 16, 38, 39, 59, and 179 formed a highly supported clade (100% bootstrap and 1.0 posterior probability values), which was closely related to ULC46.

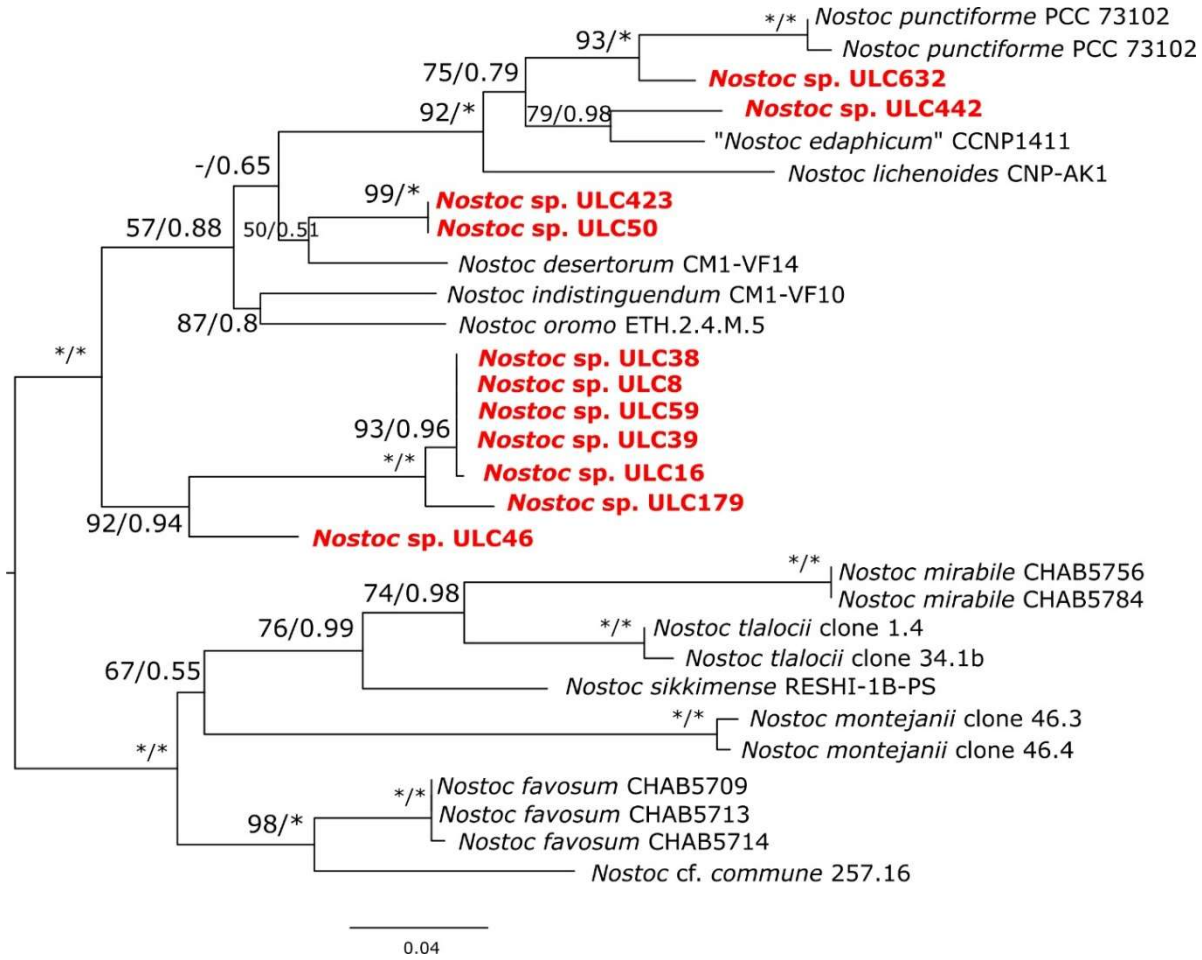

Figure 13. Maximum Likelihood (ML) phylogenetic tree based on the complete 16S−23S ITS region sequences of the studied strains together with closely related taxa. Node labels indicate bootstrap values (≥50%) and posterior probabilities (≥0.50) derived from Maximum Likelihood and Bayesian analyses, respectively. Bootstrap values of 100% or posterior probabilities of 1.00 are marked with an asterisk (*), whereas bootstrap values <50% or posterior probabilities <0.50 are indicated with a dash (–). Studied species are highlighted in bold red font. GenBank accession numbers are given in parentheses. The scale bar represents 0.04 substitutions per nucleotide position.

For the studied ULC strains that fell within the *Nostoc sensu stricto* clade, ITS percent dissimilarity values were also calculated (Table 3), ULC strains 8, 38, 39, 50, 59 and 179 shared 0−2.89% dissimilarity with each other and 7.91−21.85% dissimilarity values with the remaining ULC strains and validly described *Nostoc* species. Likewise, ULC strains 50 and 423 shared 0% dissimilarity values with each other, 6.41% dissimilarity with *N. desertorum* CM1-VF14 and more than 8% dissimilarity with the remaining *Nostoc* species. ULC442 shared 4.86% dissimilarity with *N. edaphicum* CCNP1411 whereas ULC632 shared 5.48–6.20% dissimilarity values with *N. punctiforme* PCC 73102 ITS regions.

Considering the secondary structure, in all *Nostoc* strains (including ULC strains), the D1-D1' helices were 67–71 nucleotides (nt) long and the most common length was 67 nt (Appendix 6). As seen in Figure 14, the hypothetical secondary structures obtained for D1 stem region are relatively conserved. ULC strains 8, 16, 38, 39, 50, 59, 423 had identical primary and secondary structures. The D1 stem of these strains was characterized by a 6 bp-long basal stem, followed by a 7-residue asymmetrical internal loop, a 3-residue stem, a 3-residue asymmetrical internal loop, a 5 bp stem, 1-residue left bulge, a 4 bp stem and a 5-residue terminal hairpin. Likewise, the D1 stem of ULC632 was identical to *N. desertorum* CM1-VF14 and *N. indistinguendum* CM1-VF10 in terms of both primary and secondary structures and structurally identical to ULC strains 8, 16, 38, 39, 50, 59, 423. The D1-D1' helices of ULC46 and 442 as well as *N. oromo*, *N. punctiforme* PCC 73102, *N. sikkimense* RESHI-1B-PS, "*N. edaphicum*" CCNP1411, *N. jammuense* (2JNA-PS and 21A-PS) and *N. globosum* 4CHA-PS, were structurally identical with the ULC strains mentioned above but had differences in their primary structures. The D1 stem of ULC179 was structurally identical to *N. lichenoides* CNP-AK1, *N. mirabile* (strains CHAB 5784 and 5756) and *N. breve* BG11-PS. When compared to ULC strains 8, 16, 38, 39, 50, 59, 423, the D1-D1' helices of ULC179 and other strains in this group had an identical basal stem and middle part. The only difference observed between these groups is the presence of a 3-residue asymmetrical internal loop followed by a 3 bp long stem, instead of a 1-residue left bulge that was followed by a 4 bp long stem. The symmetrical internal loop in the subterminal region and the terminal hairpin were also observed in ULC179 and the remaining *Nostoc* spp. of this group. The D1 stem of remaining strains *N. commune* 257-16, *N. coriaceum* 34TNA-PS, *N. favosum* CHAB 5709, *N. montejanii*, and *N. tlalocii* varied greatly in both primary and secondary structures.

Table 3. *Percent dissimilarity matrix of the 16S−23S rRNA sequence among our studied strains and related taxa*

Strain ID and name	**8**	**16**	**38**	**39**	**46**	**50**	**59**	**179**	**423**	**442**	**632**
8	–										
16	0,19	–									
38	0,00	0,19	–								
39	0,00	0,19	0,00	–							
59	0,00	0,19	0,00	0,00	–						
46	7,91	8,00	7,91	7,91	7,91	–					
179	2,60	2,89	2,60	2,60	2,60	9,18	–				
50	13,80	13,61	13,80	13,80	13,80	9,73	14,89	–			
423	13,80	13,61	13,80	13,80	13,80	9,73	14,89	0,00	–		
442	16,88	17,45	16,88	16,88	16,88	14,31	17,32	10,97	10,97	–	
632	16,59	15,93	16,59	16,59	16,59	13,82	16,79	9,54	9,54	7,13	–
*Nostoc_cf_commune*_257_16	16,91	17,58	16,91	16,91	16,91	15,91	15,46	19,22	19,22	15,78	17,95
*Nostoc_punctiforme*_PCC_73102	17,46	16,82	17,46	17,46	17,46	14,99	17,42	13,06	13,06	9,84	5,48
*Nostoc_punctiforme*_PCC_73102_2	17,94	17,31	17,94	17,94	17,94	15,47	17,90	13,51	13,51	10,62	6,20
*Nostoc_indistinguendum*_CM1_VF10	14,28	14,60	14,28	14,28	14,28	10,43	14,92	9,34	9,34	14,22	13,54
*Nostoc_lichenoides*_CNP_AK1	20,60	20,58	20,60	20,60	20,60	16,44	20,56	12,95	12,95	11,38	10,62
*Nostoc_desertorum*_CM1_VF14	12,16	12,16	12,16	12,16	12,16	8,88	12,81	6,41	6,41	11,05	9,59
*Nostoc_edaphicum*_CCNP1411	16,60	16,67	16,60	16,60	16,60	13,37	16,84	10,98	10,98	4,86	7,78
*Nostoc_oromo*_ETH_2_4_M_5	12,56	12,83	12,56	12,56	12,56	9,42	12,99	8,24	8,24	9,88	11,77
*Nostoc_favosum*_CHAB5709	16,34	16,99	16,34	16,34	16,34	14,37	16,76	18,02	18,02	15,78	15,78
*Nostoc_favosum*_CHAB5713	16,34	16,99	16,34	16,34	16,34	14,37	16,76	18,02	18,02	15,78	15,78
*Nostoc_favosum*_CHAB5714	16,82	17,24	16,82	16,82	16,82	14,85	17,23	18,25	18,25	16,26	16,25
*Nostoc_mirabile*_CHAB5756	19,23	18,68	19,23	19,23	19,23	17,30	19,44	16,99	16,99	14,58	17,02
*Nostoc_mirabile*_CHAB5784	19,23	18,68	19,23	19,23	19,23	17,30	19,44	16,99	16,99	14,58	17,02
*Nostoc_montejanii*_clone_46_3	18,51	18,93	18,51	18,51	18,51	17,74	17,49	21,51	21,51	20,26	19,90
*Nostoc_montejanii*_clone_46_4	18,15	18,55	18,15	18,15	18,15	17,37	17,14	21,12	21,12	19,87	19,52
*Nostoc_tlalocii*_clone_1_4	17,76	17,69	17,76	17,76	17,76	16,20	19,18	17,83	17,83	16,06	16,76
*Nostoc_tlalocii*_clone_34_1b	17,34	17,24	17,34	17,34	17,34	15,74	18,77	17,16	17,16	15,85	16,56
*Nostoc_sikkimense*_RESHI_1B_PS	18,63	18,29	18,63	18,63	18,63	16,21	18,10	17,49	17,49	16,70	14,18

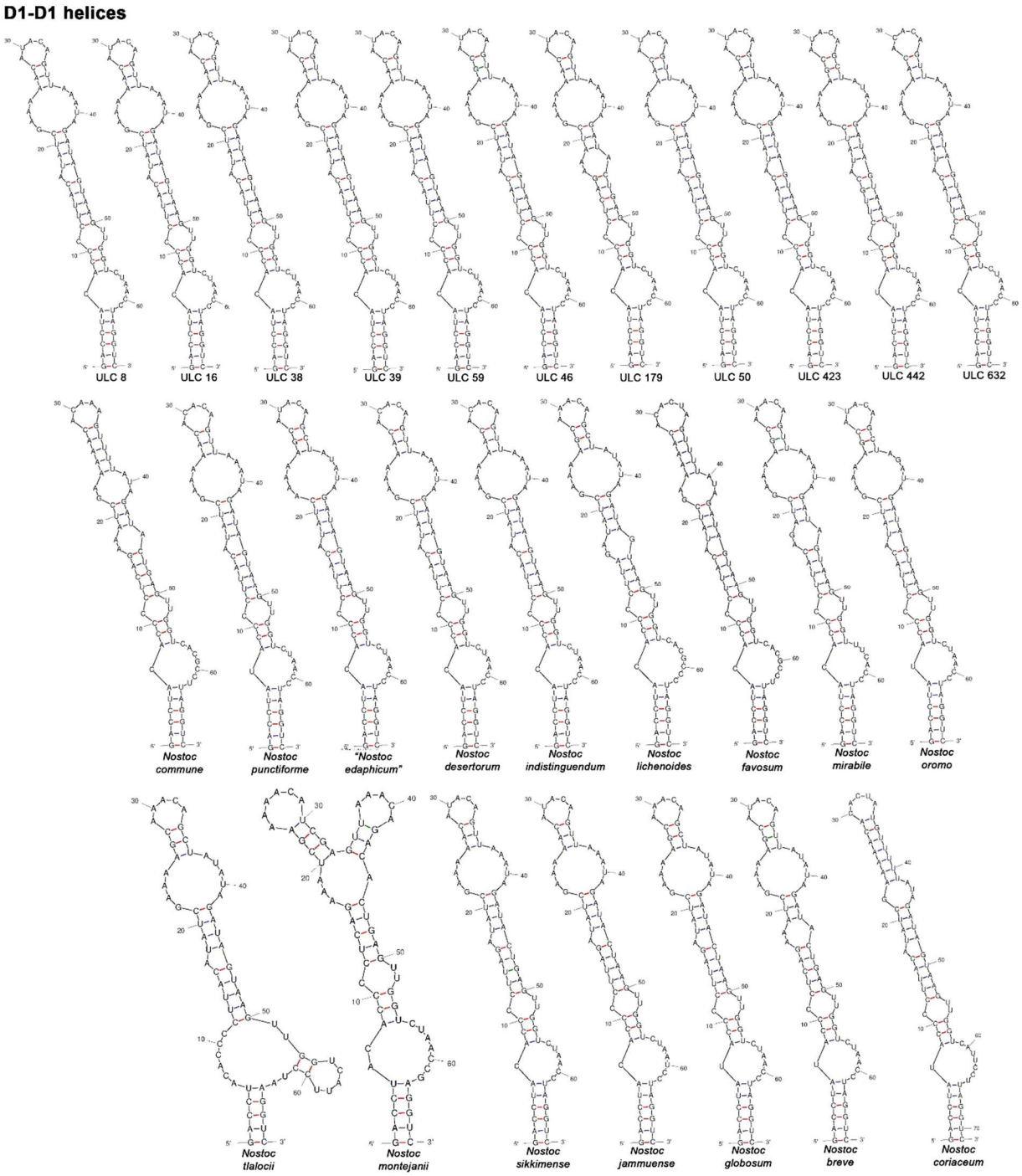

Figure 14. ITS folded structures of the D1–D1' helices in the studied strains and in closely related *Nostoc sensu stricto* species, all of which contain both tRNA genes.

Box B domains of all strains examined in this study were 27−34 nucleotides long (Appendix 6). As seen in Figure 15, all strains had a conserved 4 bp-long basal stem and a 6-residue symmetrical

internal loop but differed on their subterminal and terminal regions (4−6 bp-long basal stem and a 3−6 nt long terminal hairpin). ULC strains 8, 16, 38, 39, 59 and 632 were identical to each other in both primary and secondary structures. They were characterized by a 4 bp-long basal stem and a 6-residue symmetrical internal loop followed by a 5 bp-long stem region and a 4 nt long terminal hairpin. These strains were structurally identical to ULC423, *N. commune* 257-16, *N. globosum* 4CHA-PS, *N. oromo, N. tlalocii* and *N. breve* BG11-PS. The primary and secondary structures of ULC 50 and 423 were identical to each other and structurally identical to *N. sikkimense* RESHI-1B-PS, *N. desertorum* CM1-VF14 and *N. indistinguendum* CM1-VF10, *N. lichenoides* CNP-AK1. Here, the conserved parts were followed by a 6 bp-long stem region and a 5 nt long terminal hairpin instead of a 5 bp-long stem region and a 4 nt long terminal hairpin observed in the previous group of strains (ULC 8, 16, 38, 39, 59, 632). In ULC46 the conserved parts were followed by a 4 bp-long stem region and a 5 nt long terminal hairpin whereas in ULC179, the symmetrical internal loop was followed by a 6 bp-long stem region and a 3 nt long terminal hairpin. It is worth noting that the box B secondary structures of ULC 46 and 179 were unique among the ULC strains and the remaining *Nostoc* species. Furthermore, "*N. edaphicum*" CCNP1411 and *N. jammuense* (2JNA-PS and 21A-PS) were structurally identical. They differ from other studied strains by having a 6 bp-long stem region and a 4 nt long terminal hairpin. Moreover *N. coriaceum* 34TNA-PS, *N. favosum* CHAB 5709 and *N. montejanii* were structurally identical to each other while *N. punctiforme* PCC 73102 and *N. mirabile* (strains CHAB 5784 and 5756) had unique box B structures.

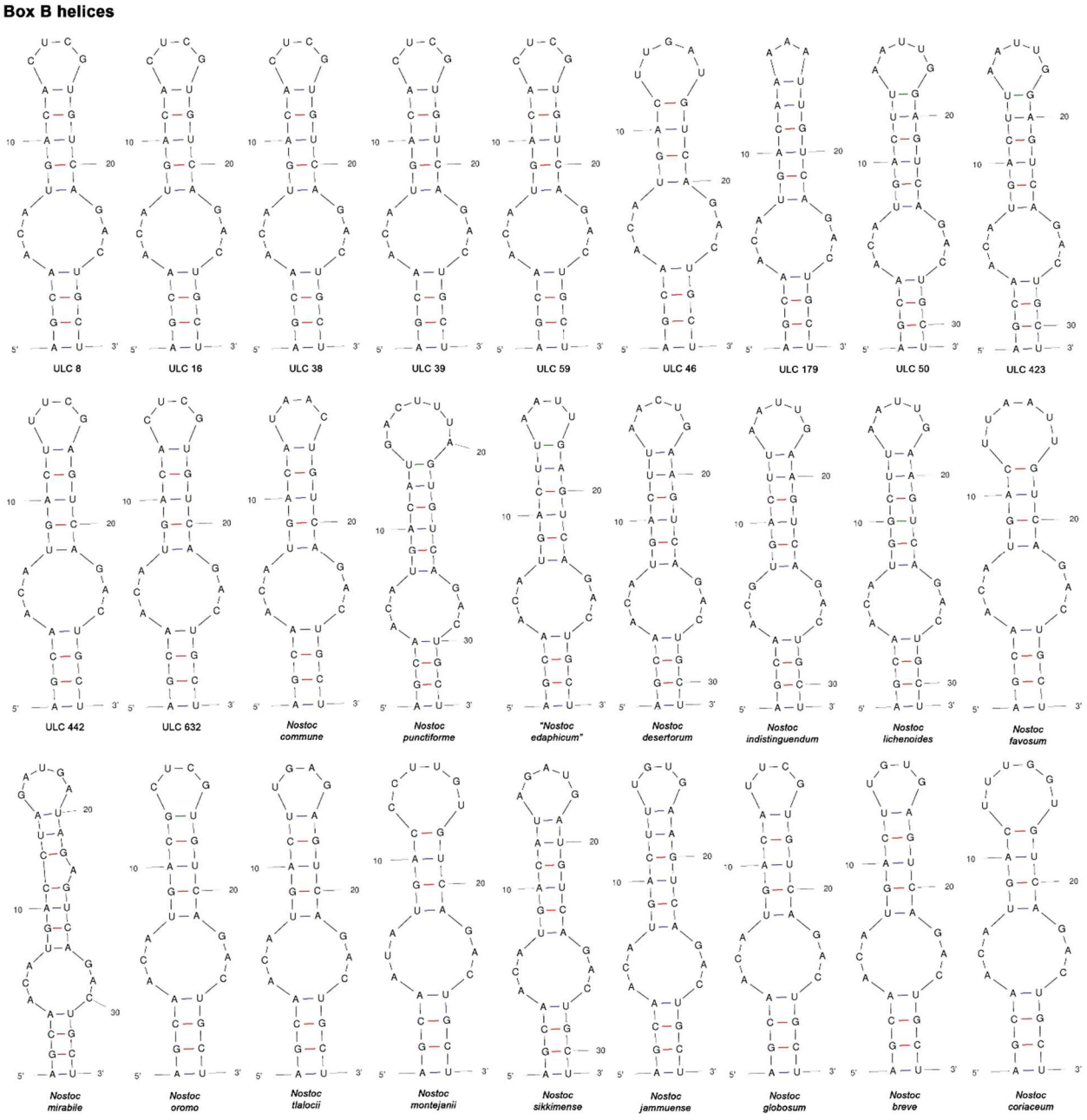

Figure 15. ITS folded structures of the box B helices in the studied strains and in closely related *Nostoc sensu stricto* species, all of which contain both tRNA genes.

The V3 region was the most variable compared to D1 and box B helices. The length of V3 ranged between 25-106 nucleotides (Appendix 6). As seen in Figure 16, ULC 8, 16, 38, 39, 46, 59, and 179 shared identical primary and secondary structures. ULC50, ULC423 and *Nostoc desertorum* CM1-VF14 were identical to each other and structurally identical to ULC 8, 16, 38, 39, 46, 59, and

179. The V3 helix of *N. jammuense* (2JNA-PS and 21A-PS) was structurally identical to ULC 8, 16, 38, 39, 46, 59, and 179 too. All these strains were characterized by a conserved basal stem (11 bp-long), an asymmetrical internal loop, a 4 bp-long stem region and a 4 nt long terminal hairpin. Unlike all other ULC strains that had 39 nt long V3 helices, ULC442 and ULC632 had longer V3 helices (106 nt long) and unique folded structures. None of the remaining studied *Nostoc* strains exhibited similar V3 secondary folded structures with the studied ULC strains.

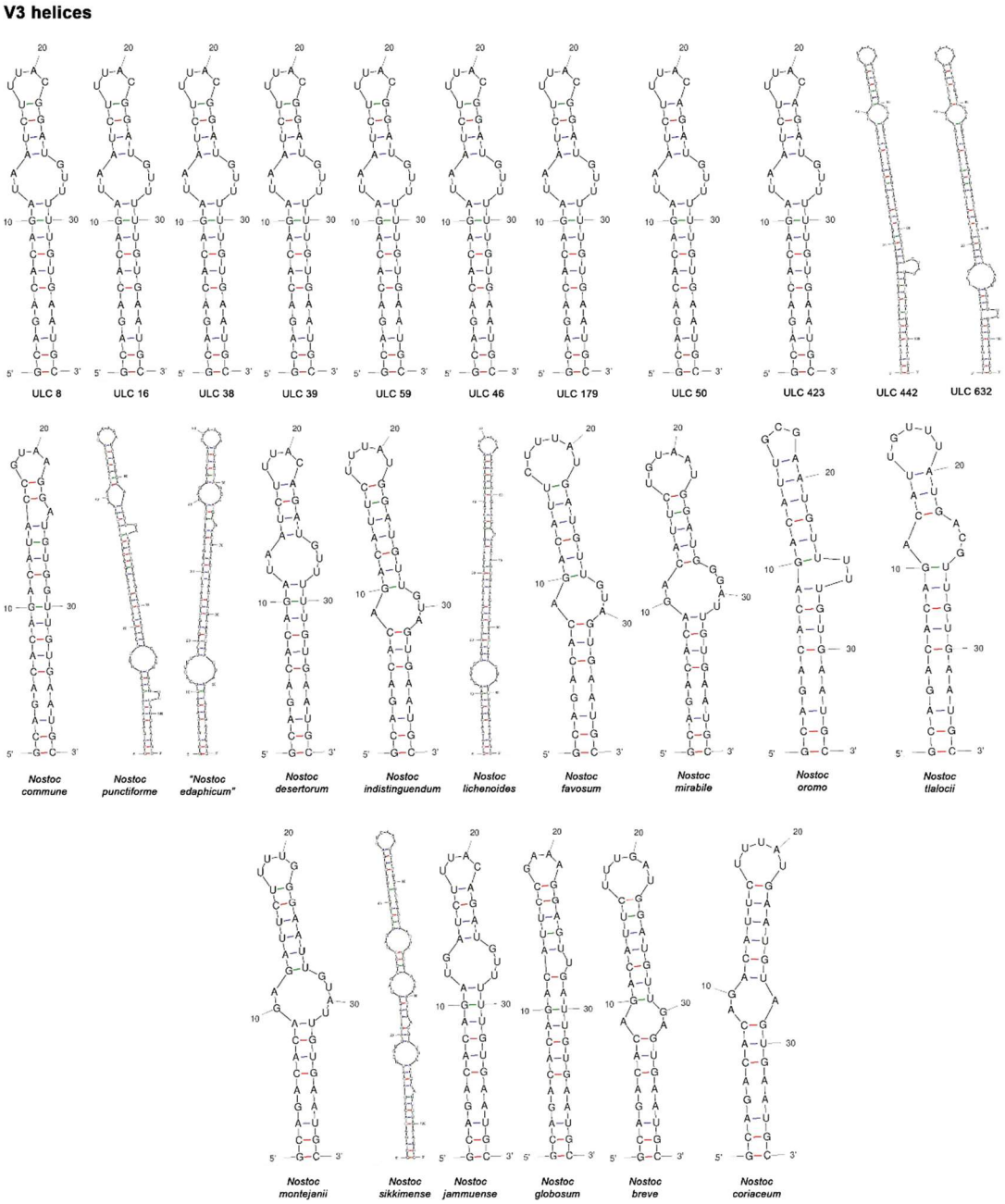

Figure 16. ITS folded structures of the V3 helices in the studied strains and in closely related *Nostoc sensu stricto* species, all of which contain both tRNA genes.

The conserved ITS domains of ULC619 (Fig. 17) which most likely represents a new nostocalean genus within were compared to its closely related genera *Halotia*, *Kryptousia*, and *Spirirestis*. The D1 stem region of ULC619 differed from the remaining genera. D1 helix was characterized by a 6 bp-long basal stem followed by a 7-residue asymmetrical internal loop, a mid-helix part with 3 internal loops and a 5 nt long terminal hairpin. The box B was characterized by a 4 bp-long basal stem, a 6-residue symmetrical internal loop, a 4 bp-long stem region and a 5 nt long terminal hairpin. Interestingly, the box B secondary folded structure of ULC619, was identical to the box B helix of ULC46. The V3 helix of ULC619 had no structural similarity with the studied genera; it was characterized by a 10 bp basal stem and a 5-residue terminal hairpin.

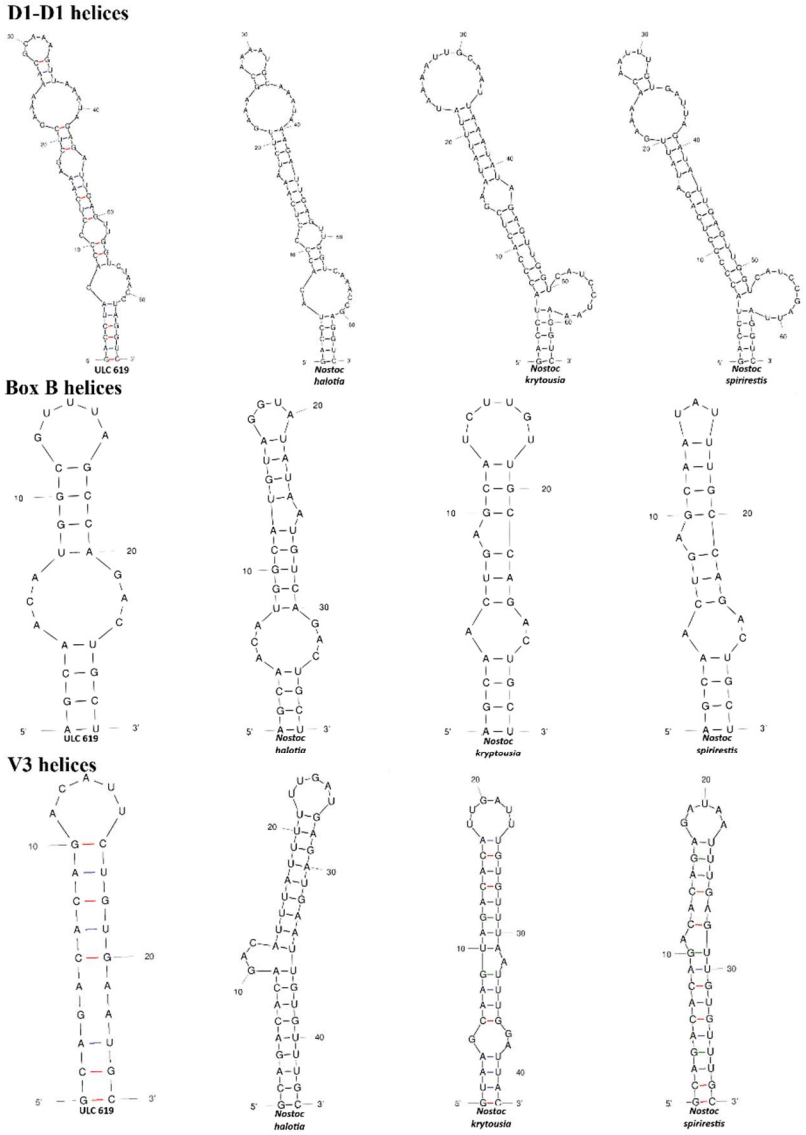

Figure 17. Comparative secondary structure analysis of the D1–D1′, BoxB, and V3 helices of ULC619 and closely related genera within the Nostocaceae.

3.2.6 Combined analysis

The combined 16S rRNA + ITS phylogeny (Fig. 18) is highly similar in topology to the ITS tree, retaining one cluster that includes our studied isolates together with the corresponding validly described *Nostoc* species. In contrast, a second cluster composed solely of reference taxa shows some rearrangements compared to the ITS tree. In the combined tree, ULC632 clustered tightly with *N. punctiforme* PCC 73102, while ULC442 grouped with *N. edaphicum* CCNP1411. ULC423 clustered with ULC50 in proximity to *N. desertorum* CM1-VF14. Furthermore, ULC38, ULC39, ULC59, ULC8, and ULC16 formed a coherent subclade that was closely related to ULC179. ULC46 was placed within the same clade but on a separate branch.

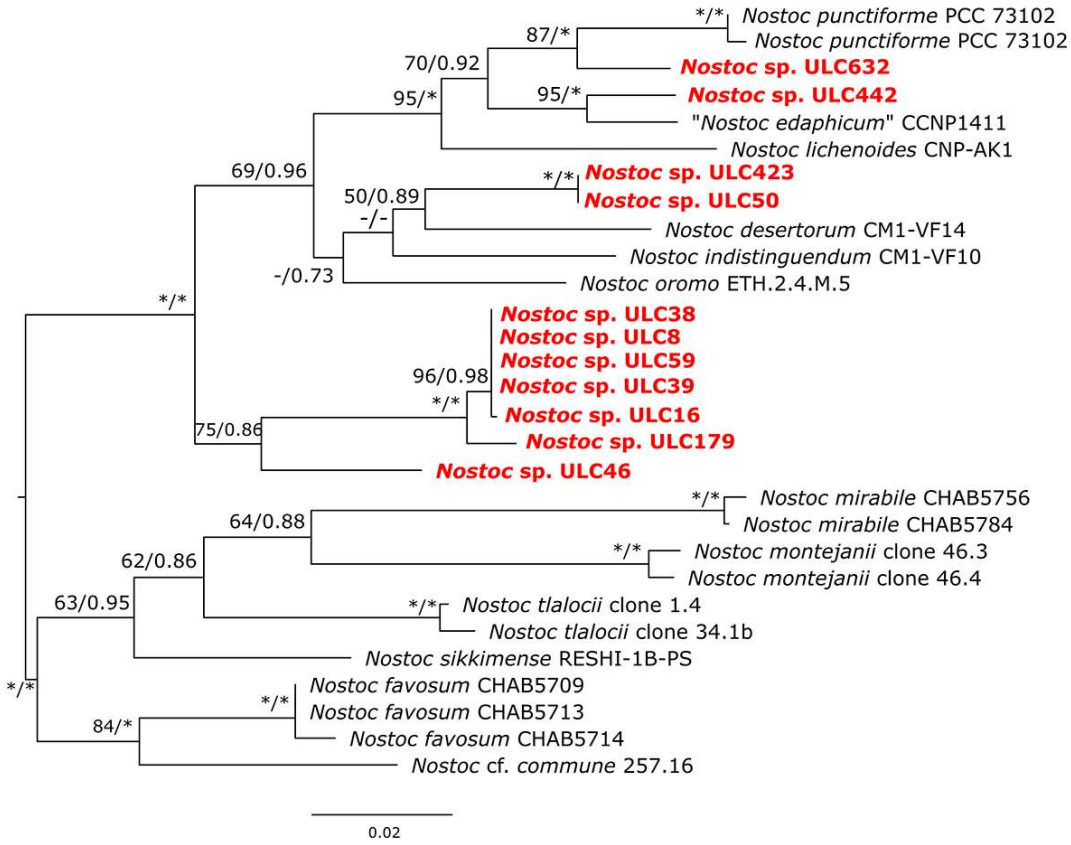

Figure 18. Maximum Likelihood (ML) phylogenetic tree based on 16S rRNA + 23S ITS region sequences of the studied strains together with closely related taxa. Node labels indicate bootstrap values (≥50%) and posterior probabilities (≥0.50) derived from Maximum Likelihood and Bayesian analyses, respectively. Bootstrap values of 100% or posterior probabilities of 1.00 are marked with an asterisk (*), whereas bootstrap values <50% or posterior probabilities <0.50 are indicated with a dash (–). Studied species are highlighted in bold red font. GenBank accession numbers are given in parentheses. The scale bar represents 0.02 substitutions per nucleotide position.

4 Discussion

This study applied a polyphasic approach to characterize cyanobacterial strains isolated from both Antarctic and European ecosystems. The results indicate the presence of cryptic diversity, with several strains likely representing novel species within the *Nostoc sensu stricto* clade, and a novel genus closely related to *Nostoc*.

4.1 DNA quality and PCR performance

Genomic DNA yields (22.5–60.5 ng/µL) and the broad range of $A_{260/280}$ and $A_{260/230}$ values (1.4–1.8 and 0.8–3.6, respectively), indicate variable extraction purity across samples (Table 2). Nevertheless, amplification success for 16S rRNA, and ITS markers, and the consistent obtention of expected amplicon sizes (~1200 bp for 16S rRNA; and 16S–23S ITS bands near ~500 and ~750–800 bp) demonstrate that the DNA was suitable for further molecular work. In contrast, strain ULC169 had consistently poor chromatograms with multiple superimposed peaks for all targeted markers. This is likely due to a mixture of organisms being co-amplified. For this reason, ULC169 was not further studied. This highlights the critical importance of good isolation techniques and culture purity as essential requirements for a reliable polyphasic taxonomy.

4.2 Molecular taxonomic markers: 16S rRNA and ITS sequences

In this study, 16S rRNA gene phylogenetic analysis confirms the placement of eleven strains (i.e., ULC8, ULC16, ULC38, ULC39, ULC46, ULC50, ULC59, ULC179, ULC423, ULC442, and ULC632) within the *Nostoc sensu stricto* clade, with sequence similarities to other members of the clade exceeding the 94.5% threshold proposed by Yarza et al., (2014) for genus delineation. However, strain ULC619, although showing similarities above this threshold (95.7– 96.9%) forms a distinct clade in the 16S rRNA phylogenetic tree with uncultured Nostocales, suggesting a potential novel genus closely related to *Nostoc sensu stricto*, but requiring further investigation.

Moreover, the 16S rRNA gene sequence similarity among the studied *Nostoc* strains ranged from 97.83 to 100%. Some of these values exceed the proposed 98.7–99% threshold for species

delineation (Stackebrand & Ebers, 2006). Specifically, strains in **Groups 1** (ULC8, ULC16, ULC38, ULC39, ULC59, ULC179) and **2** (ULC50, ULC423) showed 100% intra-group similarity, while still sharing 98.70–99.54% similarity with multiple describes species, including 11 references for **Group 1** and 4 for **Group 2**, (e.g., *N. edaphicum* X and *N. sikkimense* RESHI-1B-PS, proposed as isotype of the species (Pal et al., 2025)). Similarly, ULC442 and ULC632 shared 98.7% similarity with each other and exceeded the proposed threshold with other described species such as *N. punctiforme* PCC73102, *N. jammuense* 2JNA-PS, and *N. breve* BG11-PS, further highlighting the limited resolution of the 16S rRNA gene for species-level taxonomy in *Nostoc* and supports the need for more variable molecular markers (Bohunická et al., 2015; Fox et al., 1992). The limited resolution of the 16S rRNA gene for species delineation observed in this study has been previously reported in diverse cyanobacterial genera including *Roholtiella*, and *Pseuedanabaena* (Bohunická et al., 2015; Christodoulou et al., 2023).

For this study, we applied both ITS secondary structure analysis and percent dissimilarity calculations to resolve the taxonomic uncertainties remaining after 16S rRNA gene analysis. However, publicly available ITS sequences for certain reference species (including *N. coriaceum*, *N. globosum*, and *N. breve*) were excluded from the analysis due to their short length, which made them unsuitable for reliable comparison.

According to established thresholds (Erwin & Thacker, 2008), ITS sequence dissimilarity values of 0-3% suggest conspecificity, values between 3-7% fall within an ambiguous range requiring additional phenotypic support, while values exceeding 7% provide strong evidence for distinct species. Our analysis revealed 0-0.19% dissimilarity among strains of **Group 1** (ULC8, ULC16, ULC38, ULC39, ULC59, and ULC179), confirming their status as a single distinct species. Similarly, **Group 3** (ULC423 and ULC50) showed 0% dissimilarity, supporting their classification as a single, distinct species. And **Group 2** (ULC46) showed >7% dissimilarity with all *Nostoc* strains.

However, some ITS dissimilarity values fall within the ambiguous range, including 4.86% (ULC442 vs. *N. edaphicum* CCNP1411), 5.48–6.20% (ULC632 vs. *N. punctiforme* PCC73102), and 6.41% (**Group 3** vs. *N. desertorum* CM1-VF14), which necessitates further investigation.

Therefore, the secondary structures of the ITS region, specifically the D1-D1', Box-B, and V3 helices, were analyzed to provide an independent analysis. The D1-D1' region was the most

conserved among all the studied regions, followed by Box-B. For example, the D1-D1' region featured an identical 6 bp basal stem across all strains. This high degree of conservation in the D1-D1' architecture aligns with patterns observed in other cyanobacterial genera (Christodoulou et al., 2023).

In contrast, the V3 region exhibited the most significant structural variation, particularly in distinguishing strains with ambiguous sequence dissimilarity values. ULC442 and ULC632 each possessed unique V3 secondary-structure architectures that are absent in *N.* edaphicum CCNP1411 and *N. punctiforme* PCC73102, respectively, providing strong, independent evidence for treating each of them as distinct species despite intermediate sequence dissimilarity.

On the other hand, although **Group 1** (ULC8, ULC16, ULC38, ULC39, ULC59, and ULC179) and **Group 3** (ULC50 and ULC423) shared a simple, identical V3 structure, they differed in their Box-B secondary structure. However, **Group 3** (ULC423, ULC50) also showed the same D1-D1', Box-B, and V3 secondary structures as *N. desertorum* CM1-VF14, which necessitates the integration of morphology and ecology to confirm their similarities.

This integrated approach demonstrates that secondary structure analysis is indispensable for resolving taxonomic uncertainties that arise when relying solely on sequence dissimilarity values within *Nostoc*, but it also requires morphological and ecological evidence to confirm phylogenetic relationships.

4.3 Comparative analysis of morphological and ecological features

The genus *Nostoc* represents a widespread morphologically complex group of cyanobacteria, thriving in a remarkable diversity of freshwater, terrestrial, and extreme environments (Komárek, 2013). Moreover, in all the studied strains, there was an overlap in the narrow trichomes' dimensions with width ranges between 2.91-5.26 micrometers. Nevertheless, a comparative morphological analysis of the studied cyanobacterial strains revealed distinct groupings. **Group 1** (ULC8, ULC16, ULC38, ULC39, ULC59, ULC179) includes strains with a planktonic to benthic habit, forming non-attached clusters of long, flexuous, and constricted trichomes at the bottom of the culture vessel. Internal variability was observed in the consistent production of akinetes and occasional motility, but the overall trichome structure and growth mode support their grouping.

Group 2 (ULC46) and **Group 3** (ULC50, ULC423) share an attached, membranous biofilm with microcolonies surrounded by mucilage. They are distinguished from one another mainly by trichomes width, with **Group 3** showing consistently broader trichomes and cylindrical cells, in contrast to the narrower trichomes of **Group 2**. **Group 4** (ULC442) differs from all previous groups by its subaerophytic growth and a characteristic developmental pattern where entire trichomes gradually enlarge and differentiate into akinetes during senescence. Finally, **Group 5** (ULC632) stands apart as a unique morphotype, characterized by the formation of a thick, brown-pigmented mucilaginous mat and by the presence of rare oval heterocytes, a combination not observed in any other strain.

In addition, by comparing our strains to published *Nostoc* species and to the flora by Komárek, (2013), it was shown that: **Group 1** shows the strongest morphological convergence with *N. sikkimense* (N. Kumar et al., 2024) in its benthic origin, long flexuous and irregularly coiled trichomes, and constricted cross-walls. However, it differs by its strictly planktonic growth and the absence of both macroscopic and microcolony formation.

Group 2 closely aligns with *N. tlalocii* (Carmona Jiménez et al., 2023) in its ontogeny, forming spherical microcolonies through filament entanglement with mucilage compartmentalization, yet remaining microscopic and never developing the macroscopic ear-shaped colonies typical of *N. tlalocii*. A major divergence is ecological, with group 2 originating from an Antarctic microbial mat, in contrast to the high-current stream habitat of *N. tlalocii* in Mexico.

Group 3 shares the wide trichomes of biofilm-forming species such as *N. desertorum* (Řeháková et al., 2007), but does not produce their macroscopic aggregated colonies. Its Antarctic mat origin further distinguishes it from the sandy desert soil habitats of *N. desertorum*.

Group 4 shares a subaerophytic habit and ontogenetic strategy with soil *Nostoc*, but forms a thin, membranous thallus and lacks the well-defined spherical colonies characteristic of species such as *N. edaphicum* (Komárek, 2013).

Group 5, although geographically overlapping with *N. punctiforme* (Komárek, 2013), differs by forming a submerged mat rather than the macroscopic spherical to confluent blackish gelatinous masses (up to several cm) typical of subaerophytic *N. punctiforme*. It also diverges from *N.*

commune (Komárek, 2013), which develops macroscopic, firm, and crispy colonies not observed in group 5.

While occupying similar ecological niches to *N. antarcticum* (Komárek, 2013), the studied strains never formed macroscopic colonies visible to the naked eye, unlike the distinct pale blue-green colonies described for that species.

4.4 Application of polyphasic approach

Therefore, the taxonomic conclusions of this study are based on the integration of molecular phylogenetic data with morphological and ecological characteristics (i.e., polyphasic approach). Based on these criteria, six groups were distinguished: five represent novel species, and one represents a novel genus.

Group 1 (ULC8, ULC16, ULC38, ULC39, ULC59, and ULC179); the 16S rRNA gene, ITS sequence and combined phylogenetic analyses placed these strains within a single clade. They are characterized by 0–0.19% ITS sequence dissimilarity and identical secondary structures for the D1-D1', Box-B, and V3 helices, as well as an identical morphological characteristic (i.e, long, flexuous trichomes with pronounced constrictions at cross-walls and a strictly planktonic growth habit in culture). However, the high 16S rRNA gene sequence similarity to other species (98.70–99.54%; e.g., to *N. commune* EV1-KK1 and *N. sikkimense* RESHI-1B-PS) is misleading, as it is contradicted by their distinct ecology and clear ITS based separation. The strains planktonic lifestyle, absence of microcolony formation, and formation of free-floating clusters represent a significant ecological divergence from the benthic, colonial, or soil-associated habitats of their phylogenetic neighbors. This ecological and developmental distinction, supported by the ITS and combined analyses' distinction, confirms that the high 16S rRNA similarity reflects the conserved nature of this gene rather than true taxonomic identity, which supports the recognition of strains of Group 1 as a novel species.

Group 2 (ULC46); phylogenetic analysis based on the 16S rRNA gene placed this strain near *N. tlalocii*, with high sequence similarity suggesting a potential relationship. However, this initial molecular signal is contradicted by finer-scale analysis. The ITS analysis revealed both sequence dissimilarity and distinct D1-D1', Box-B, and V3 helices, which differentiate ULC46 from *N.*

tlalocii. Morphologically, while both share the trait of forming spherical microcolonies, ULC46 is distinguished by its consistently narrower trichome width and its formation of only microscopic structures, whereas *N. tlalocii* is characterized by macroscopic ear-shaped colonies. This morphological divergence is further supported by a major ecological difference: Group 2 originates from an Antarctic microbial mat, in contrast to the tropical high-current stream habitat of *N. tlalocii*. Thus, the high 16S rRNA gene similarity is contradicted by the combined evidence from ITS structure, detailed morphology, and ecology, indicating that ULC46 represents a distinct polar species.

Group 3 (ULC50, ULC423); these strains share 100% 16S rRNA gene sequence similarity and 0% dissimilarity across their 16S–23S ITS region. This genetic identity is further reflected in their identical secondary structures for the D1-D1', Box-B, and V3 helices, providing strong molecular evidence that they represent a single phylogenetic species.

While the 16S rRNA gene placed them in close similarity to several described species (e.g., *N. punctiforme* and *N. edaphicum*), the ITS region differentiated them from these taxa. Notably, it revealed a 6.41% dissimilarity between Group 3 and *N. desertorum*, a value that falls within the ambiguous range for species delineation. This molecular ambiguity was further reinforced by the fact that the 16S–23S ITS secondary structures of the D1-D1', Box-B, and V3 helices were identical to those of *N. desertorum*. Morphologically, this clade is characterized by a consistent phenotype of wide trichomes that form biofilms. While this resembles *N. desertorum*, it diverges in lacking the production of macroscopic aggregated colonies. This molecular and morphological ambiguity is decisively resolved by ecology: the Antarctic microbial mat origin of Group 3 is fundamentally different from the sandy desert soil habitat that defines *N. desertorum*. Thus, the combination of all these criteria provides strong evidence for recognizing this clade as a novel species, distinct from *N. desertorum*.

Group 4 (ULC442) is delineated by unique molecular and phenotypic autapomorphies. Based on the 16S rRNA gene, it clusters within the same species as ULC632; however, 16S–23S ITS dissimilarity values do not support this, instead revealing a 4.86% dissimilarity with *N. edaphicum* CCNP1411, a value that falls within the ambiguous range for species separation. This ambiguity is resolved by its secondary structures, which display a distinct Box-B configuration compared to *N. edaphicum* and a unique V3 structure not observed in *N. edaphicum* or any other strains.

Morphologically, it shares a subaerophytic habit and ontogenetic strategy with *N. edaphicum*, but differs by forming a thin, membranous thallus and lacking the well-defined spherical colonies characteristic of *N. edaphicum*. These combined molecular and morphological features support its recognition as a novel species.

Group 5 (ULC632) shows high 16S rRNA similarity with all the groups described above, except for Group 2, and with *N. punctiforme*. However, ITS dissimilarity analysis indicates that it is distinct from all other groups, falling within the ambiguous range (5.48–6.20%) with *N. punctiforme*. Its secondary structures, however, provide definitive evidence of divergence, possessing a distinct Box-B and a uniquely extended V3 fold that is structurally distinct from *N. punctiforme* and all other strains. Morphologically, it is characterized by a brown-pigmented mucilaginous mat and by the production of rare, oval-shaped heterocytes. Ecologically, its formation of a submerged mat in Antarctica contrasts with the subaerophytic, macroscopic gelatinous colonies of *N. punctiforme*. Thus, the combination of molecular, morphological, and ecological features supports its recognition as a novel species.

Group 6 (ULC619); the 16S rRNA similarity analysis and the morphological characters shows that this strain belongs to the genus *Nostoc*. However, the 16S rRNA phylogenetic tree places it in a separate clade together with uncultured Nostocales cyanobacteria, and the ITS secondary structure further demonstrates that it is not structurally identical to *Nostoc*, nor to other members of this Nostocales cluster. The inability of the 16S rRNA gene to resolve generic relationships is not surprising, as several studies have shown that the ~95% similarity threshold is too low for Nostocales, and the morphology alongside the phylogenetic tree topologies should be considered (Bohunická et al., 2015; Hentschke et al., 2016; Kaštovský et al., 2014; Responses & Scales, 2012). Thus, ULC619 should be considered as a new genus.

5 Conclusion and perspectives

This polyphasic study clarified the taxonomic position of the investigated *Nostoc* strains and showed that they fall into five separate groups within the *Nostoc sensu stricto* clade.
The integration of 16S rRNA gene phylogeny, 16S–23S ITS sequence dissimilarity and secondary structure analysis, and detailed morphological and ecological characterization

provided a strong basis for species distinction.

The 16S rRNA gene sequence proved unreliable for separation at the species level, and the proposed thresholds for genus and species delineation should likely be more restrictive. The 16S–23S ITS region provided greater resolution, with secondary structures of the D1-D1', Box-B, and V3 helices offering precise diagnostic characters; i.e., strains with ambiguous ITS sequence dissimilarity values (3–7%) were definitively classified through their unique secondary structures, along with morphological and ecological traits, that proved to be necessary for a definitive conclusion.

Group 1 (ULC8, ULC16, ULC38, ULC39, ULC59, ULC179) is confirmed as a novel species, distinguished by its planktonic ecology despite high 16S rRNA similarity to benthic species.

Group 2 (ULC46) represents a novel species, differentiated from *N. tlalocii* by its morphology and Antarctic habitat.

Group 3 (ULC50, ULC423) is identified as a novel species, with ecology as the definitive distinguishing factor from *N. desertorum*.

Group 4 (ULC442) and **Group 5** (ULC632) are established as two novel species based on their unique molecular characteristics in ITS secondary structures and distinctive morphologies.

Notably, **Group 6** (ULC619) represents a novel genus, as its unique ITS secondary structures, especially the distinct V3 helix architecture, differentiate it from both *Nostoc sensu stricto* and the uncultured Nostocales cyanobacteria with which it clusters phylogenetically, despite its morphological resemblance to classical *Nostoc*.

The exclusion of strain ULC169 from the analysis due to poor sequence quality highlights the importance of careful isolation and culture purity in taxonomic studies. Furthermore, the inability to include certain reference species due to poor-quality public sequences highlights an ongoing challenge in cyanobacterial taxonomy.

In conclusion, this work is an example of the necessity of a polyphasic approach for accurate species separation in the genus *Nostoc*, effectively overcoming the limitations of single-marker analysis or morphology alone. For future perspectives, studies could include the formal taxonomic description of the proposed novel taxa. Additionally, more genetic markers, or even whole-genome sequencing, could be applied to provide stronger phylogenetic resolution.

Bibliography

Adams, D. G., & Duggan, P. S. (2008). Cyanobacteria-bryophyte symbioses. *Journal of Experimental Botany*, *59*(5), 1047–1058. https://doi.org/10.1093/jxb/ern005

Akaike, H. (1974). A new look at the statistical model identification. *IEEE Transactions on Automatic Control*, *19*(6), 716–723. https://doi.org/10.1109/TAC.1974.1100705

Altschul, S. F., Gish, W., Miller, W., Myers, E. W., & Lipman, D. J. (1990). Basic local alignment search tool. *Journal of Molecular Biology*, *215*(3), 403–410. https://doi.org/10.1016/S0022-2836(05)80360-2

Alvarenga, D. O., Andreote, A. P. D., Branco, L. H. Z., Delbaje, E., Cruz, R. B., Varani, A. de M., & Fiore, M. F. (2021). Amazonocrinis nigriterrae gen. nov., sp. nov., Atlanticothrix silvestris gen. nov., sp. nov. and Dendronalium phyllosphericum gen. nov., sp. nov., nostocacean cyanobacteria from Brazilian environments. *International Journal of Systematic and Evolutionary Microbiology*, *71*(5). https://doi.org/10.1099/ijsem.0.004811

Ashelford, K. E., Chuzhanova, N. A., Fry, J. C., Jones, A. J., & Weightman, A. J. (2005). At least 1 in 20 16S rRNA sequence records currently held in public repositories is estimated to contain substantial anomalies. *Applied and Environmental Microbiology*, *71*(12), 7724–7736. https://doi.org/10.1128/AEM.71.12.7724-7736.2005

Bagchi, S. N., Dubey, N., & Singh, P. (2017). Phylogenetically distant clade of Nostoc-like taxa with the description of Aliinostoc gen. Nov. and Aliinostoc morphoplasticum sp. nov. *International Journal of Systematic and Evolutionary Microbiology*, *67*(9), 3329–3338. https://doi.org/10.1099/ijsem.0.002112

Bekker, A., Holland, H. D., Wang, P.-L., Rumble, D., Stein, H. J., Hannah, J. L., Coetzee, L. L., & Beukes, N. J. (2004). Dating the rise of atmospheric oxygen. *Nature*, *427*(6970), 117–120. https://doi.org/10.1038/nature02260

Biondi, N., Tredici, M. R., Taton, A., Wilmotte, A., Hodgson, D. A., Losi, D., & Marinelli, F. (2008). Cyanobacteria from benthic mats of Antarctic lakes as a source of new bioactivities. *Journal of Applied Microbiology*, *105*(1), 105–115. https://doi.org/10.1111/j.1365-2672.2007.03716.x

Bohunická, M., Pietrasiak, N., Johansen, J. R., Gómez, E. B., Hauer, T., Gaysina, L. A., & Lukešová, A. (2015). Roholtiella, gen. nov. (Nostocales, Cyanobacteria)—a tapering and branching cyanobacteria of the family Nostocaceae. *Phytotaxa*, *197*(2), 84. https://doi.org/10.11646/phytotaxa.197.2.2

Boyer, S. L., Flechtner, V. R., & Johansen, J. R. (2001). Is the 16S-23S rRNA internal transcribed spacer region a good tool for use in molecular systematics and population genetics? A case study in cyanobacteria. *Molecular Biology and Evolution*, *18*(6), 1057–1069. https://doi.org/10.1093/oxfordjournals.molbev.a003877

Cai, F., & Li, R. (2020). Purpureonostoc, a new name for a recently described genus of nostoc-like cyanobacteria. *Fottea*, *20*(2), 111. https://doi.org/10.5507/fot.2020.007

Cai, F., Li, X., Geng, R., Peng, X., & Li, R. (2019). Phylogenetically distant clade of Nostoc-like taxa with the description of Minunostoc gen. nov. and Minunostoc cylindricum sp. nov. *Fottea*, *19*(1), 13–24. https://doi.org/10.5507/fot.2018.013

Cai, F., Li, X., Yang, Y., Jia, N., Huo, D., & Li, R. (2019). Compactonostoc shennongjiaensis gen . & sp. nov . (Nostocales, Cyanobacteria) from a wet rocky wall in China. *Phycologia*, *58*(2), 200–210. https://doi.org/10.1080/00318884.2018.1541270

Cai, F., Peng, X., & Li, R. (2020). Violetonostoc minutum gen. et sp. nov. (nostocales, cyanobacteria) from a rocky substrate in China. *Algae*, *35*(1), 1–15. https://doi.org/10.4490/algae.2020.35.3.4

Cai, F., Wang, Y., Yu, G., Wang, J., Peng, X., & Li, R. (2020). Proposal of purpurea gen. Nov. (nostocales, cyanobacteria), a novel cyanobacterial genus from wet soil samples in Tibet, China. *Fottea*, *20*(1), 86–97. https://doi.org/10.5507/fot.2019.018

Carmona Jiménez, J., Caro Borrero, A., Becerra-Absalón, I., Perona Urizar, E., Márquez Santamaría, K., & Mateo Ortega, P. (2023). Description of two new species of Nostoc (Nostocales, Cyanobacteria) from central Mexico, using morphological, ecological, and molecular attributes. *Journal of Phycology*, *59*(6), 1237–1257. https://doi.org/10.1111/jpy.13401

Casamatta, D. A., Johansen, J. R., Vis, M. L., & Broadwater, S. T. (2005). Molecular and morphological characterization of ten polar and near-polar strains within the oscillatoriales (Cyanobacteria). *Journal of Phycology*, *41*(2), 421–438. https://doi.org/10.1111/j.1529-8817.2005.04062.x

Casamatta, D. A., Villanueva, C. D., Garvey, A. D., Stocks, H. S., Vaccarino, M., Dvořák, P., Hašler, P., & Johansen, J. R. (2020). Reptodigitus Chapmanii (Nostocales, Hapalosiphonaceae) Gen. Nov.: A Unique Nostocalean (Cyanobacteria) Genus Based on a Polyphasic Approach1. *Journal of Phycology*, *56*(2), 425–436. https://doi.org/10.1111/jpy.12954

Christodoulou, M., Jokela, J., Wahlsten, M., Saari, L., Economou-Amilli, A., Fiore, M. de F., & Sivonen, K. (2022). Description of Aliinostoc alkaliphilum sp. nov. (Nostocales, Cyanobacteria), a New Bioactive Metabolite-Producing Strain from Salina Verde (Pantanal, Brazil) and Taxonomic Distribution of Bioactive Metabolites in Nostoc and Nostoc-like Genera. *Water*, *14*(16), 2470. https://doi.org/10.3390/w14162470

Christodoulou, M., Wahlsten, M., & Sivonen, K. (2023). Morphological and Molecular Evaluation of Pseudanabaena epilithica sp. nov. and P. suomiensis sp. nov. (Pseudanabaenaceae, Cyanobacteria) from Finland. *Diversity*, *15*(8), 909. https://doi.org/10.3390/d15080909

Cordeiro, R., Luz, R., Vasconcelos, V., Gonçalves, V., & Fonseca, A. (2020). Cyanobacteria Phylogenetic Studies Reveal Evidence for Polyphyletic Genera from Thermal and Freshwater Habitats. *Diversity*, *12*(8), 298. https://doi.org/10.3390/d12080298

Cornet, L., Ahn, A. C., Wilmotte, A., & Baurain, D. (2021). Orper: A workflow for constrained ssu rrna phylogenies. *Genes*, *12*(11). https://doi.org/10.3390/genes12111741

Cornet, L., Wilmotte, A., Javaux, E. J., & Baurain, D. (2018). A constrained SSU-rRNA phylogeny reveals the unsequenced diversity of photosynthetic Cyanobacteria (Oxyphotobacteria). *BMC Research Notes*, *11*(1). https://doi.org/10.1186/s13104-018-3543-y

Cuddy, W. S., Neilan, B. A., & Gehringer, M. M. (2012). Comparative analysis of cyanobacteria in the rhizosphere and as endosymbionts of cycads in drought-affected soils. *FEMS Microbiology Ecology*, *80*(1), 204–215. https://doi.org/10.1111/j.1574-6941.2011.01288.x

Darriba, D., Taboada, G. L., Doallo, R., & Posada, D. (2012). jModelTest 2: more models, new heuristics and parallel computing. *Nature Methods*, *9*(8), 772. https://doi.org/10.1038/nmeth.2109

Demoulin, C. F., Lara, Y. J., Cornet, L., François, C., Baurain, D., Wilmotte, A., & Javaux, E. J. (2019). Cyanobacteria evolution: Insight from the fossil record. *Free Radical Biology and Medicine*, *140*, 206–223. https://doi.org/10.1016/j.freeradbiomed.2019.05.007

Dextro, R. B., Andreote, A. P. D., Vaz, M. G. M. V., Carvalho, C. R., & Fiore, M. F. (2024). The pros and cons of axenic cultures in cyanobacterial research. *Algal Research*, *78*(November 2023), 103415. https://doi.org/10.1016/j.algal.2024.103415

Dextro, R. B., Delbaje, E., Cotta, S. R., Zehr, J. P., & Fiore, M. F. (2021). Trends in Free-access Genomic Data Accelerate Advances in Cyanobacteria Taxonomy. *Journal of Phycology*, *57*(5), 1392–1402. https://doi.org/10.1111/jpy.13200

Dodds, W. K., Gudder, D. A., & Mollenhauer, D. (1995). THE ECOLOGY OF NOSTOC. *Journal of Phycology*, *31*(1), 2–18. https://doi.org/10.1111/j.0022-3646.1995.00002.x

Doolittle, W. F. (1988). Bacterial evolution. *Canadian Journal of Microbiology*, *34*(4), 547–551. https://doi.org/10.1139/m88-093

Dvořák, P., Hindák, F., Hašler, P., Hindáková, A., & Poulíčková, A. (2014). Morphological and molecular studies of Neosynechococcus sphagnicola, gen. et sp. nov. (Cyanobacteria, Synechococcales). *Phytotaxa*, *170*(1), 24–34. https://doi.org/10.11646/phytotaxa.170.1.3

Dvořák, P., Jahodářová, E., Casamatta, D. A., Hašler, P., & Poulíčková, A. (2018). Difference without distinction? Gaps in cyanobacterial systematics; when more is just too much. *Fottea*, *18*(1), 130–136. https://doi.org/10.5507/fot.2017.023

Dvořák, P., Poulíčková, A., Hašler, P., Belli, M., Casamatta, D. A., & Papini, A. (2015). Species concepts and speciation factors in cyanobacteria, with connection to the problems of diversity and classification. *Biodiversity and Conservation*, *24*(4), 739–757. https://doi.org/10.1007/s10531-015-0888-6

Erwin, P. M., & Thacker, R. W. (2008). Cryptic diversity of the symbiotic cyanobacterium Synechococcus spongiarum among sponge hosts. *Molecular Ecology*, *17*(12), 2937–2947. https://doi.org/10.1111/j.1365-294X.2008.03808.x

Fox, G. E., Wisotzkey, J. D., & Jurtshuk, P. (1992). How close is close: 16S rRNA sequence identity may not be sufficient to guarantee species identity. *International Journal of Systematic Bacteriology*, *42*(1), 166–170. http://www.ncbi.nlm.nih.gov/pubmed/1371061

Garduño-Solórzano, G., Martínez-García, M., Hentschke, G. S., Miguel Solorza, L. F., & Vasconcelos, V. M. (2024). A phylogenetically distant clade of Nostoc–like (Cyanobacteria) taxa with the description of Reofilinostoc matlalcueyense gen. et sp. nov. from an extreme environment. *Phytotaxa*, *655*(2), 125–143. https://doi.org/10.11646/phytotaxa.655.2.2

Geitler, L. (1932). Cyanophyceae. In A. Pascher (Ed.), *Rabenhorst's Kryptogamen-Flora von Deutschland, Österreich und der Schweiz,Zweite Auflage, Band 14*. Akademische Verlagsgesellschaft. https://bibdigital.rjb.csic.es/records/item/10392-rabenhorst-s-kryptogamen-flora-zweite-auflage-band-14

Genuário, D., Vaz, M., Hentschke, G., Sant'Anna, C., & Fiore, M. (2015). Halotia gen. nov., a phylogenetically and physiologically coherent cyanobacterial genus isolated from marine coastal environments. *International Journal of Systematic and Evolutionary Microbiology*, *65*(2), 633–675. https://doi.org/10.1099/ijs.0.070078-0

Glez-Peña, D., Gómez-Blanco, D., Reboiro-Jato, M., Fdez-Riverola, F., & Posada, D. (2010). ALTER: Program-oriented conversion of DNA and protein alignments. *Nucleic Acids Research*, *38*(SUPPL. 2), 14–18. https://doi.org/10.1093/nar/gkq321

Hentschke, G. S., Johansen, J. R., Pietrasiak, N., Fiore, M. de F., Rigonato, J., Anna, C. L. S., & Komárek, J. (2016). Phylogenetic placement of Dapisostemon gen. nov. and Streptostemon, two tropical heterocytous genera (Cyanobacteria). *Phytotaxa*, *245*(2), 129–143. https://doi.org/10.11646/phytotaxa.245.2.4

Hentschke, G. S., Johansen, J. R., Pietrasiak, N., Rigonato, J., Fiore, M. F., & Sant'Anna, C. L. (2017). Komarekiella atlantica gen. Et sp. nov. (nostocaceae, cyanobacteria): A new subaerial taxon from the Atlantic rainforest and Kauai, Hawaii. *Fottea*, *17*(2), 178–190. https://doi.org/10.5507/fot.2017.002

Hoffmann Lucien, Komarek Jiri, & Kastovsky Jan. (2004). System of cyanoprokaryotes (cyanobacteria) - state in 2004. *Algological Studies*, 95–115. https://doi.org/0342-1120/05/0159-095

Hrouzek, P., Lukešová, A., Mareš, J., & Ventura, S. (2013). Description of the cyanobacterial genus Desmonostoc gen. nov. including D. muscorum comb. nov. as a distinct, phylogenetically coherent taxon related to the genus Nostoc. *Fottea*, *13*(2), 201–213. https://doi.org/10.5507/fot.2013.016

Iteman, I., Rippka, R., Tandeau de Marsac, N., & Herdman, M. (2000). Comparison of conserved structural and regulatory domains within divergent 16S rRNA–23S rRNA spacer sequences of cyanobacteria The GenBank accession numbers for the sequences reported in this paper are AF180968 and AF180969 for ITS-L and ITS-S, respective. *Microbiology*, *146*(6), 1275–1286. https://doi.org/10.1099/00221287-146-6-1275

Johansson, C., Johansson, C., Soderback, E., & Soderback, E. (1992). Tansley Review No. 42 The Nostoc—Gunner a symbiosis. *Review Literature And Arts Of The Americas*, *42*, 379–400.

Jungblut, A. D. (2022). Ecology and Biogeography of the Cyanobacteria. In *Bergey's Manual of Systematics of Archaea and Bacteria* (pp. 1–11). Wiley. https://doi.org/10.1002/9781118960608.bm00037

Kaštovský, J., Gomez, E. B., Hladil, J., & Johansen, J. R. (2014). Cyanocohniella calida gen. et sp. nov. (cyanobacteria: Aphanizomenonaceae) a new cyanobacterium from the thermal springs from Karlovy Vary, Czech Republic. *Phytotaxa*, *181*(5), 279–292. https://doi.org/10.11646/phytotaxa.181.5.3

Komarek, J. (2006). Cyanobacterial Taxonomy: Current Problems and Prospects for the Integration of Traditional and Molecular Approaches. *ALGAE*, *21*(4), 349–375. https://doi.org/10.4490/ALGAE.2006.21.4.349

Komárek, J. (2010a). Modern taxonomic revision of planktic nostocacean cyanobacteria: A short review of genera. *Hydrobiologia*, *639*, 231–243. https://doi.org/10.1007/s10750-009-0030-4

Komárek, J. (2010b). Recent changes (2008) in cyanobacteria taxonomy based on a combination of molecular background with phenotype and ecological consequences (genus and species concept). *Hydrobiologia*, *639*(1), 245–259. https://doi.org/10.1007/s10750-009-0031-3

Komárek, J. (2013). *Cyanoprokaryota – 3. Teil / 3rd Part: Heterocytous Genera* (M. S. (Eds. . B. Büdel, G. Gärtner, L. Krienitz (ed.)). Springer Spektrum.

Komárek, J. (2016). A polyphasic approach for the taxonomy of cyanobacteria: principles and applications. *European Journal of Phycology*, *51*(3), 346–353. https://doi.org/10.1080/09670262.2016.1163738

Komárek, J. (2020). Quo vadis, taxonomy of cyanobacteria (2019). *Fottea*, *20*(1), 104–110. https://doi.org/10.5507/fot.2019.020

Komárek, J., & Kaštovský, J. (2003). Coincidences of structural and molecular characters in evolutionary lines of cyanobacteria. *Algological Studies/Archiv Für Hydrobiologie, Supplement Volumes*, *109*(August 2003), 305–325. https://doi.org/10.1127/1864-1318/2003/0109-0305

Komárek, J., Kaštovský, J., Mareš, J., & Johansen, J. R. (2014). Taxonomic classification of cyanoprokaryotes (cyanobacterial genera) 2014, using a polyphasic approach. *Preslia*, *86*, 295–335.

Kumar, N., Saraf, A., Pal, S., & Singh, P. (2024). Expanding the cyanobacterial flora of India: Multiple novel species of Nostoc and Desmonostoc from Jammu and Kashmir, India using a polyphasic approach. *Journal of Phycology*, *60*(5), 1190–1209. https://doi.org/10.1111/jpy.13498

Kumar, S., Stecher, G., & Tamura, K. (2016). MEGA7: Molecular Evolutionary Genetics Analysis Version 7.0 for Bigger Datasets. *Molecular Biology and Evolution*, *33*(7), 1870–1874. https://doi.org/10.1093/molbev/msw054

Kurmayer, R., Sivonen, K., Wilmotte, A., & Salmaso, N. (Eds.). (2017). *Molecular Tools for the Detection and Quantification of Toxigenic Cyanobacteria*. Wiley. https://doi.org/10.1002/9781119332169

Lamprinou, V., Skaraki, K., Kotoulas, G., Economou-Amilli, A., & Pantazidou, A. (2012). Toxopsis calypsus gen. nov., sp. nov. (Cyanobacteria, Nostocales) from cave “Francthi”, Peloponnese, Greece: A morphological and molecular evaluation. *International Journal of Systematic and Evolutionary Microbiology*, *62*(12), 2870–2877.

https://doi.org/10.1099/ijs.0.038679-0

Lane, D. . (1991). 16S/23S rRNA sequencing. In E. Stackebrandt & M. Goodfellow (Eds.), *Nucleic Acid Techniques in Bacterial Systematics* (pp. 115–175). John Wiley & Sons, Inc.

Larkin, M. A., Blackshields, G., Brown, N. P., Chenna, R., Mcgettigan, P. A., McWilliam, H., Valentin, F., Wallace, I. M., Wilm, A., Lopez, R., Thompson, J. D., Gibson, T. J., & Higgins, D. G. (2007). Clustal W and Clustal X version 2.0. *Bioinformatics*, *23*(21), 2947–2948. https://doi.org/10.1093/bioinformatics/btm404

Lee, N.-J., Bang, S.-D., Kim, T., Ki, J.-S., & Lee, O.-M. (2021). Pseudoaliinostoc sejongens gen. & sp. nov. (Nostocales, Cyanobacteria) from floodplain soil of the Geum River in Korea based on polyphasic approach. *Phytotaxa*, *479*(1), 55–70. https://doi.org/10.11646/phytotaxa.479.1.4

Lowe, T. M., & Chan, P. P. (2016). tRNAscan-SE On-line: integrating search and context for analysis of transfer RNA genes. *Nucleic Acids Research*, *44*, W54–W57. https://doi.org/10.1093/nar/gkw413

Martineau, E., Wood, S. A., Miller, M. R., Jungblut, A. D., Hawes, I., Webster-Brown, J., & Packer, M. A. (2013). Characterisation of Antarctic cyanobacteria and comparison with New Zealand strains. *Hydrobiologia*, *711*(1), 139–154. https://doi.org/10.1007/s10750-013-1473-1

Mesfin, M., JOHANSEN, J. R., PIETRASIAK, N., & BALDARELLI, L. M. (2020). Nostoc oromo sp. nov. (Nostocales, Cyanophyceae) from Ethiopia: a new species based on morphological and molecular evidence. *Phytotaxa*, *433*(2), 81–93. https://doi.org/10.11646/phytotaxa.433.2.1

Muñoz-Martín, M. Á., Becerra-Absalón, I., Perona, E., Fernández-Valbuena, L., Garcia-Pichel, F., & Mateo, P. (2019). Cyanobacterial biocrust diversity in Mediterranean ecosystems along a latitudinal and climatic gradient. *New Phytologist*, *221*(1), 123–141. https://doi.org/10.1111/nph.15355

Nguyen, L.-T., Schmidt, H. A., von Haeseler, A., & Minh, B. Q. (2015). IQ-TREE: A fast and effective stochastic algorithm for estimating Maximum-Likelihood phylogenies. *Molecular Biology and Evolution*, *32*(1), 268–274. https://doi.org/10.1093/molbev/msu300

Nowruzi, B., Hutarova, L., Ševelenyiova, D., & Metcalf, J. S. (2024). Characterization of Neowestiellopsis persica A1387 (Hapalosiphonaceae) based on the cpcA, psbA, rpoC1, nifH and nifD gene sequences. *BMC Ecology and Evolution*, *24*(1), 1–14. https://doi.org/10.1186/s12862-024-02244-z

Nübel, U., Garcia-Pichel, F., & Muyzer, G. (1997). PCR primers to amplify 16S rRNA genes from cyanobacteria. *Applied and Environmental Microbiology*, *63*(8), 3327–3332. https://doi.org/10.1128/aem.63.8.3327-3332.1997

Pal, S., Pant, H., Kumar, N., Priya, Singh, S., Gupta, N., & Singh, P. (2025). Life on the rocks: polyphasic evaluation of three epilithic cyanobacterial strains isolated from a single rock, with the description of Nostoc sikkimense sp. nov., from the northeastern region of India. *FEMS Microbiology Letters*, *372*(February). https://doi.org/10.1093/femsle/fnaf037

Palenik, B. (1994). Cyanobacterial community structure as seen from RNA polymerase gene sequence analysis. *Applied and Environmental Microbiology*, *60*(9), 3212–3219. https://doi.org/10.1128/aem.60.9.3212-3219.1994

Palinska, K. A., & Surosz, W. (2014). Taxonomy of cyanobacteria: A contribution to consensus approach. *Hydrobiologia*, *740*(1), 1–11. https://doi.org/10.1007/s10750-014-1971-9

Pham, H. T. L., Ngo, T. T., Tran, T. V., Duong, T. A., Tran, L. D., Tran, A. T. T., Nguyen, V. T. H., & Nguyen, S. V. (2025). Classification of Nostoc-like cyanobacteria isolated from paddy soil into Aliinostoc, Aulosira, and Desmonostoc. *Frontiers in Microbiology*, *16*(May), 1–18. https://doi.org/10.3389/fmicb.2025.1581725

Potts M. (1997). Etymology of the Genus Name Nostoc (Cyanobacteria). *International Journal of Systematic Bacteriology*, *47*(2), 584–584. https://doi.org/10.1099/00207713-47-2-584

Pushkareva, E., Pessi, I. S., Namsaraev, Z., Mano, M. J., Elster, J., & Wilmotte, A. (2018). Cyanobacteria inhabiting biological soil crusts of a polar desert: Sør Rondane Mountains, Antarctica. *Systematic and Applied Microbiology*, *41*(4), 363–373. https://doi.org/10.1016/j.syapm.2018.01.006

Rajaniemi, P., Hrouzek, P., Kaštovská, K., Willame, R., Rantala, A., Hoffmann, L., Komárek, J., & Sivonen, K. (2005). Phylogenetic and morphological evaluation of the genera Anabaena, Aphanizomenon, Trichormus and Nostoc (Nostacales, cyanobacteria). *International Journal of Systematic and Evolutionary Microbiology*, *55*(1), 11–26. https://doi.org/10.1099/ijs.0.63276-0

Rambaut, A. (2007). *FigTree*. https://doi.org/http://tree.bio.ed.ac.uk/software/figtree/

Raymond, J. A., Janech, M. G., & Mangiagalli, M. (2021). Ice-Binding Proteins Associated with an Antarctic Cyanobacterium, Nostoc sp. HG1. *Applied and Environmental Microbiology*, *87*(2), e02499-20. https://doi.org/10.1128/AEM.02499-20

Řeháková, K., Johansen, J. R., Casamatta, D. A., Xuesong, L., & Vincent, J. (2007). Morphological and molecular characterization of selected desert soil cyanobacteria: Three species new to science including Mojavia pulchra gen. et sp. nov. *Phycologia*, *46*(5), 481–502. https://doi.org/10.2216/06-92.1

Responses, P., & Scales, D. (2012). Phytoplankton responses to human impacts at different scales. In N. Salmaso, L. Naselli-Flores, L. Cerasino, G. Flaim, M. Tolotti, & J. Padisák (Eds.), *Phytoplankton responses to human impacts at different scales*. Springer Netherlands. https://doi.org/10.1007/978-94-007-5790-5

Richmond, A. (Ed.). (2003). *Handbook of Microalgal Culture*. Wiley. https://doi.org/10.1002/9780470995280

Rikkinen, J. (2013). Molecular studies on cyanobacterial diversity in lichen symbioses. *MycoKeys*, *6*(May), 3–32. https://doi.org/10.3897/mycokeys.6.3869

Rippka, R. (1988). *Isolation and purification of cyanobacteria* (pp. 3–27). https://doi.org/10.1016/0076-6879(88)67004-2

Risser, D. D. (2023). Hormogonium Development and Motility in Filamentous Cyanobacteria.

Applied and Environmental Microbiology, *89*(6). https://doi.org/10.1128/aem.00392-23

Rocap, G., Distel, D. L., Waterbury, J. B., & Chisholm, S. W. (2002). Resolution of Prochlorococcus and Synechococcus ecotypes by using 16S-23S ribosomal DNA internal transcribed spacer sequences. *Applied and Environmental Microbiology*, *68*(3), 1180–1191. https://doi.org/10.1128/AEM.68.3.1180-1191.2002

Roncero-Ramos, B., Muñoz-Martín, M. Á., Chamizo, S., Fernández-Valbuena, L., Mendoza, D., Perona, E., Cantón, Y., & Mateo, P. (2019). Polyphasic evaluation of key cyanobacteria in biocrusts from the most arid region in Europe. *PeerJ*, *2019*(1). https://doi.org/10.7717/peerj.6169

Ronquist, F., Teslenko, M., van der Mark, P., Ayres, D. L., Darling, A., Höhna, S., Larget, B., Liu, L., Suchard, M. A., & Huelsenbeck, J. P. (2012). MrBayes 3.2: Efficient Bayesian Phylogenetic Inference and Model Choice Across a Large Model Space. *Systematic Biology*, *61*(3), 539–542. https://doi.org/10.1093/sysbio/sys029

Rudi, K., Skulberg, O. M., Larsen, F., & Jakobsen, K. S. (1997). Strain characterization and classification of oxyphotobacteria in clone cultures on the basis of 16S rRNA sequences from the variable regions V6, V7, and V8. *Applied and Environmental Microbiology*, *63*(7), 2593–2599. https://doi.org/10.1128/aem.63.7.2593-2599.1997

Sambrook, J. & Russell, D. W. (2001). *Molecular cloning : a laboratory manual* (3rd ed.). Cold Spring Harbor Laboratory Press.

Sand-Jensen, K. (2014). Ecophysiology of gelatinous Nostoc colonies: unprecedented slow growth and survival in resource-poor and harsh environments. *Annals of Botany*, *114*(1), 17–33. https://doi.org/10.1093/aob/mcu085

Seckbach, J., Chapman, D. J., Garbary, D., Oren, A., & Reisser, W. (2007). *Algae and Cyanobacteria Under Environmental Extremes* (pp. 781–786). https://doi.org/10.1007/978-1-4020-6112-7_42

Seo, P.-S., & Yokota, A. (2003). The phylogenetic relationships of cyanobacteria inferred from 16S rRNA, gyrB, rpoC1 and rpoD1 gene sequences. *The Journal of General and Applied Microbiology*, *49*(3), 191–203. https://doi.org/10.2323/jgam.49.191

Soares, F., Ramos, V., Trovão, J., Cardoso, S. M., Tiago, I., & Portugal, A. (2021). Parakomarekiella sesnandensis gen. et sp. nov. (Nostocales, Cyanobacteria) isolated from the Old Cathedral of Coimbra, Portugal (UNESCO World Heritage Site). *European Journal of Phycology*, *56*(3), 301–315. https://doi.org/10.1080/09670262.2020.1817568

Stackebrand, E., & Ebers, J. (2006). Taxonomic parameters revisited: tarnished gold standards. *Microbiology Today*, *33*(4), 152–155. http://scholar.google.com/scholar?hl=en&btnG=Search&q=intitle:Taxonomic+parameters+revisited:+tarnished+gold+standards#0

STACKEBRANDT, E., & GOEBEL, B. M. (1994). Taxonomic Note: A Place for DNA-DNA Reassociation and 16S rRNA Sequence Analysis in the Present Species Definition in Bacteriology. *International Journal of Systematic and Evolutionary Microbiology*, *44*(4), 846–849. https://doi.org/10.1099/00207713-44-4-846

Stanier, R. Y., & Cohen-Bazire, G. (1977). Phototrophic prokaryotes: the cyanobacteria. *Annual Review of Microbiology*, *31*(1), 225–274. https://doi.org/10.1146/annurev.mi.31.100177.001301

Stanojković, A., Skoupý, S., Škaloud, P., & Dvořák, P. (2022). High genomic differentiation and limited gene flow indicate recent cryptic speciation within the genus Laspinema (cyanobacteria). *Frontiers in Microbiology*, *13*(September), 1–13. https://doi.org/10.3389/fmicb.2022.977454

Strunecký, O., Ivanova, A. P., & Mareš, J. (2023). An updated classification of cyanobacterial orders and families based on phylogenomic and polyphasic analysis. *Journal of Phycology*, *59*(1), 12–51. https://doi.org/10.1111/jpy.13304

Taton, A., Grubisic, S., Brambilla, E., De Wit, R., & Wilmotte, A. (2003). Cyanobacterial Diversity in Natural and Artificial Microbial Mats of Lake Fryxell (McMurdo Dry Valleys, Antarctica): a Morphological and Molecular Approach. *Applied and Environmental Microbiology*, *69*(9), 5157–5169. https://doi.org/10.1128/AEM.69.9.5157-5169.2003

Taton, A., Grubisic, S., Ertz, D., Hodgson, D. A., Piccardi, R., Biondi, N., Tredici, M. R., Mainini, M., Losi, D., Marinelli, F., & Wilmotte, A. (2006). Polyphasic study of antarctic cyanobacterial strains. *Journal of Phycology*, *42*(6), 1257–1270. https://doi.org/10.1111/j.1529-8817.2006.00278.x

The Inkscape team. (2020). *The Inkscape project*.

Velichko, N. V., Rabochaya, D. E., Dolgikh, A. V., & Mergelov, N. S. (2023). Cyanobacteria in Hypolithic Horizons of Soils in the Larsemann Hills Oasis, East Antarctica. *Eurasian Soil Science*, *56*(8), 1067–1082. https://doi.org/10.1134/S1064229323600859

Vences, M., Patmanidis, S., Kharchev, V., & Renner, S. S. (2022). Concatenator, a user-friendly program to concatenate DNA sequences, implementing graphical user interfaces for MAFFT and FastTree. *Bioinformatics Advances*, *2*(1), 1–4. https://doi.org/10.1093/bioadv/vbac050

Wang, Y., Berthold, D. E., Hu, J., Lefler, F. W., Huang, I. S., & Laughinghouse, H. D. (2023). Novel diversity within Roseofilum (Desertifilaceae, Cyanobacteria) from marine benthic mats with description of four new species. *Journal of Phycology*, *59*(6), 1147–1165. https://doi.org/10.1111/jpy.13392

Whitton, B. A. (Ed.). (2012). *Ecology of Cyanobacteria II*. Springer Netherlands. https://doi.org/10.1007/978-94-007-3855-3

Willis, A., Woodhouse, J. N., Neilan, B. A., & Burford, M. A. (2022). *Comparative genomics for understanding intraspecific diversity: a case study of the cyanobacterium Raphidiopsis raciborskii*.

Wilmotte, A. (1994). Molecular Evolution and Taxonomy of the Cyanobacteria. In Bryant D. A. (Ed.), *The Molecular Biology of Cyanobacteria* (pp. 1–25). Springer Netherlands. https://doi.org/10.1007/978-94-011-0227-8_1

Wilmotte, A., & Golubic, S. (1991). Morphological and genetic criteria in the taxonomy of Cyanophyta/Cyanobacteria. *Arch. Hydrobiol./Suppl. ,92, Algol. Stud.; 64:1-24.*

Wilmotte, A., & Herdman, M. (2001). Phylogenetic Relationships Among the Cyanobacteria Based on 16S rRNA Sequences. In G. M. Garrity & R. W. Castenholz (Eds.), *Bergey's manual of systematic bacteriology.* (2nd ed., pp. 487–493). Williams & Wilkins, United States.

Wilmotte, A., Van der Auwera, G., & De Wachter, R. (1993). Structure of the 16 S ribosomal RNA of the thermophilic cyanobacterium chlorogloeopsis HTF (' mastigocladus laminosus HTF') strain PCC7518, and phylogenetic analysis. *FEBS Letters*, *317*(1–2), 96–100. https://doi.org/10.1016/0014-5793(93)81499-P

Yarza, P., Yilmaz, P., Pruesse, E., Glöckner, F. O., Ludwig, W., Schleifer, K. H., Whitman, W. B., Euzéby, J., Amann, R., & Rosselló-Móra, R. (2014). Uniting the classification of cultured and uncultured bacteria and archaea using 16S rRNA gene sequences. *Nature Reviews Microbiology*, *12*(9), 635–645. https://doi.org/10.1038/nrmicro3330

Zuker, M. (2003). Mfold web server for nucleic acid folding and hybridization prediction. *Nucleic Acids Research*, *31*(13), 3406–3415. https://doi.org/10.1093/nar/gkg595